ELSEVIER

Chemical Geology 196 (2003) 235–257

CHEMICAL GEOLOGY
INCLUDING
ISOTOPE GEOSCIENCE

www.elsevier.com/locate/chemgeo

Using platinum-group elements to investigate the origin of the Ontong Java Plateau, SW Pacific

James C. Ely, Clive R. Neal*

Department of Civil Engineering & Geological Science, University of Notre Dame, 156 Fitzpatrick Hall, Notre Dame, IN 46556, USA

Abstract

Fractionated basalts (4.5–8.9 wt.% MgO) from the islands of Malaita and Makira (San Cristobal) in the Solomon Islands represent outpourings of magma that formed the Ontong Java Plateau (OJP), SW Pacific. The origin of the OJP is explored by examining platinum-group element (PGE: Ru, Rh, Pd, Ir, Pt) abundances in these basalts. On Makira, mid-ocean ridge basalts (MORBs) and ocean island basalts (OIBs) are occasionally intercalated within the stratigraphic sequence of the OJP—the OIB-type basalts could be representative of the plume tail sequence and the MORB-type flows may be an indication of heterogeneity within the OJP source. Partial melting models indicate that the MORB-type basalts were generated from a source dominated by upper mantle material. However, they suggest that the OJP basalts and the OIB-type basalts were not generated from an exclusively upper mantle source. Our illustrative modeling shows the range of PGE compositions in these plume-generated basalts are best generated from a hybrid source that incorporates 0–0.5 wt.% of outer core material, 50% depleted upper mantle and 50–49.5% lower (primitive) mantle.

Keywords: Ontong Java Plateau; Platinum-group elements; Large igneous provinces; Core–mantle boundary; Geochemistry; Petrogenetic modeling

1. Introduction

There is a growing body of evidence suggesting that at least some plumes originate at the core–mantle boundary (CMB) (e.g., Coffin and Eldholm, 1993; Helmberger et al., 1998) and geophysical modeling suggests chemical interactions would occur across the CMB incorporating up to 6 wt.% of core material into the ascending plume (e.g., Kellogg and King, 1993; Boehler et al., 1995). Therefore, the siderophile element budget of the ascending plume should reflect any entrained outer core material. For example, interpretations of geophysical data suggest an origin of the Hawaiian plume at the CMB (e.g., Russell et al., 1998) and isotopic data (i.e., Re–Os and Pt–Os) from some plume-derived Hawaiian picrites have been interpreted as reflecting a small (≤ 1 wt.%) entrained outer core component (Brandon et al., 1998, 1999). Similar isotopic analyses of fractionated basalts have proven more difficult as Os behaves compatibly in typical basaltic fractionation sequences (e.g., Barnes et al., 1985; Brügmann et al., 1987; Puchtel and Humayun, 2001), resulting in Os abundances that are prohibitively low for Pt–Os analysis. In this paper, we examine platinum-group element (PGE) abundances

* Corresponding author. Tel.: +1-574-631-8328; fax: +1-574-631-9236.
E-mail address: neal.1@nd.edu (C.R. Neal).

0009-2541/02/$ - see front matter © 2002 Elsevier Science B.V. All rights reserved.
doi:10.1016/S0009-2541(02)00415-1

of fractionated basalts to investigate the origin of the Ontong Java Plateau (OJP), SW Pacific.

1.1. Background

The Alaska-sized Ontong Java Plateau is the world's largest "large igneous province" (LIP) and covers an area of at least 1.5 million km^2 in the southwest Pacific. The OJP is now exposed along its southern edge on the islands of Malaita, Ulawa, northern Santa Isabel and Makira (San Cristobal) in the Solomon Islands, due to the collision of the OJP with the Australian plate (Coleman and Kroenke, 1981; Petterson et al., 1999). It consists primarily of tholeiitic basalts, erupted in a submarine environment, formed by unusually large degrees of partial melting (~ 30%) followed by 30–50% fractional crystallization (Mahoney and Spencer, 1991; Mahoney et al., 1993; Neal et al., 1997). The main eruptive stage was concentrated around 122 Ma, with progressively smaller eruptions at ~ 90, ~ 62 and ~ 34 Ma (Tejada et al., 1996, 2002; Van Dyke, 2000). The OJP basalts have been divided into two isotopically and stratigraphically distinct groups: the Singgalo Formation, containing basalts with $\varepsilon_{Nd}(t) = +3.8$ to $+3.9$, $(^{206}Pb/^{204}Pb)_t = 17.71–17.85$, $(^{87}Sr/^{86}Sr)_t = 0.7040–0.7042$, and higher abundances of highly incompatible elements (relative to the Kwaimbaita Formation); and the Kwaimbaita Formation, containing basalts with $\varepsilon_{Nd}(t) = +5.4$ to $+5.6$, $(^{206}Pb/^{204}Pb)_t = 18.12–18.40$, $(^{87}Sr/^{86}Sr)_t = 0.7037–0.7039$, and lower abundances of highly incompatible elements (relative to the Singgalo Formation; see Tejada et al., 1996, 2002; Neal et al., 1997). These are geochemically identical to the A-type and C-G-type basalts, respectively, from Ocean Drilling Program (ODP) Site 807 on the northern flank of the OJP (Mahoney et al., 1993). On Makira, both geochemical groups were generated during the younger eruptive events (Van Dyke, 2000).

2. Samples and analytical methods

A total of 12 samples were analyzed for PGE contents: 10 OJP basalts (8 from Malaita and 2 from Makira), 1 mid-ocean ridge basalt (MORB)-type and ocean island basalt (OIB)-type (both from Makira) (Table 1). All samples from Malaita were erupted at ~ 122 Ma (Tejada et al., 2002). The MORB-type and OIB-type samples from Makira are stratigraphically intercalated with the OJP basalt sequence and gave $^{40}Ar–^{39}Ar$ ages of 43.9 (total fusion) and 67.1 ± 0.5 Ma (plateau), respectively, whereas the OJP basalts from Makira (both Singgalo-type) were erupted at 94.6 ± 3.5 (MATA-7) and 55.8 ± 5.2 Ma (WHTO-15) (see Table 1 for a complete list of sample ages and see Van Dyke, 2000; Tejada et al., 2002 for details). Sample locations of OJP basalts from the Solomon Islands on Malaita and Makira are described elsewhere (Petterson, 1995; Van Dyke, 2000; Tejada et al., 2002). Major and trace element data for the basalt samples are reported by Van Dyke (2000) and Tejada et al. (2002), but are reproduced here (Table 1) for completeness and ease of comparison with the PGE data. Major element contents for the basalts were quantified by XRF at the University of Hawaii following the methods of Norrish and Chappell (1977). Trace element data for the basalts were determined at the University of Notre Dame by ICP-MS following the method described in Neal (2001).

The general mineralogy of the basalts analyzed was dominantly plagioclase and clinopyroxene in a subvariolitic or intergranular to intersertal texture (MATA-3, MATA-7, SGB-11, SGB-22, SGB-25, WHTO-36). Samples KF-1, KF-32, SGB-15, and WHTO-15 exhibit a subophitic texture. Altered olivine phenocrysts (replaced by clay minerals) are present in SGB-11 (rare), SGB-22 (rare) and SGB-25 (sparse). Interstitial glass has been replaced in all samples by clay minerals. Samples ML-475 and ML-476 are very similar to each other, being fine- to medium-grained and containing large clinopyroxene crystals (up to 5 mm), plagioclase (up to 3 mm) and titanomagnetite (up to 2 mm). The modal abundance varies between these two rocks, with ML-475 being dominated by clinopyroxene, whereas ML-476 contains slightly less clinopyroxene and more titanomagnetite.

Accurate determination of PGE abundances in samples from the Solomon Islands of Malaita and Makira (Table 2) was accomplished using a cation exchange method in conjunction with standard addition as described by Ely et al. (1999) and the data reduction procedure of Ely and Neal (2002). Quantities of Hf and Ta passing through the cation exchange columns with the PGEs producing HfO^+ and TaO^+ interferences on ^{193}Ir, ^{194}Pt, ^{195}Pt, ^{196}Pt, and ^{197}Au, as described in Ely

Table 1
Major and trace element abundances of the basalts

Sample no.	SGB-11	SGB-15	KF-1	KF-32	MATA-7	WHTO-15	SGB-22	SGB-25	ML-475	ML-476	MATA-3	WHTO-36
Age (Ma)	122	122	122	122	95	59	122	122	122	122	44	65
Type	OJP-S	OJP-S	OJP-S	OJP-S	OJP-S	OJP-S	OJP-K	OJP-K	OJP-K	OJP-K	MORB	OIB
Island	Mal.	Mal.	Mal.	Mal.	Mak.	Mak.	Mal.	Mal.	Mal.	Mal.	Mak.	Mak.
SiO_2	49.1	49.4	50.1	49.7	50.3	49.4	48.9	49.0	49.7	47.9	47.1	47.6
TiO_2	1.39	1.13	1.28	1.27	1.82	1.36	0.98	0.93	0.73	2.07	1.86	2.45
Al_2O_3	14.2	14.5	14.4	15.9	14.5	14.4	14.7	14.8	14.0	13.2	14.2	17.2
Fe_2O_3	14.3	13.0	12.2	12.1	12.6	12.8	12.9	12.6	9.84	18.5	12.5	11.2
MnO	0.21	0.19	0.19	0.18	0.20	0.18	0.19	0.21	0.16	0.25	0.22	0.16
MgO	7.15	7.35	8.09	7.04	4.93	7.36	7.41	7.86	9.99	5.83	7.80	5.04
CaO	11.6	12.3	10.9	12.3	10.2	11.6	13.0	13.2	14.5	9.61	na	9.96
Na_2O	2.19	2.05	2.94	1.85	4.18	2.12	1.84	1.51	1.48	3.08	na	4.66
K_2O	0.08	0.12	0.23	0.09	0.16	0.07	0.09	0.05	0.08	0.09	na	0.74
P_2O_5	0.15	0.11	0.08	0.11	0.20	0.10	0.10	0.10	0.06	0.17	na	0.40
Li	5.4	6.4	6.5	4.8	8.3	7.7	4.2	4.6	3.5	5.2	6.2	14.8
Be	0.81	0.69	0.45	0.41	0.64	0.35	0.66	0.39	0.25	0.72	0.52	1.18
Sc	44.3	48.0	31.0	33.0	46.0	43.4	45.3	46.2	57.9	43.4	33.1	20.5
Cr	83	103	155	167	na	na	133	139	446	101	na	na
Co	48.7	51.0	55.0	55.2	50.3	47.7	52.9	52.5	38.8	52.0	35.3	45.0
Ni	55.7	71.5	96.0	91.0	51.6	74.8	88.2	97.1	133	35.0	25.5	70.4
Cu	111	128	117	120	115	115	162	156	128	174	23.7	42.2
Zn	115	96.2	70.0	72.0	157	106	97.3	96.5	47	111	92.3	131
Ga	18.0	16.9	18.4	19.9	18.8	14.9	16.2	16.3	13.1	21.5	13.9	23.2
Rb	0.46	1.35	3.31	1.62	3.43	1.29	0.97	0.46	0.91	1.45	0.37	8.3
Sr	150	136	116	138	135	353	127	126	135	129	67.6	300
Y	30.1	23.7	18.3	21.7	37.6	25.1	22.9	20.7	10.3	31.8	35.0	21.3
Zr	100	78	60	73	134	70	68	68	30	102	98	168
Nb	5.9	4.5	3.5	4.1	8.2	3.9	3.9	3.7	2.7	6.5	2.7	27.8
Cs	0.02	0.01	0.11	0.01	na	na	0.01	0.01	0.01	0.02	na	0.54
Ba	24.7	17.0	133	22.0	49.5	47.0	12.8	12.3	11.5	13.4	11.1	254
La	2.7	4.4	4.1	4.4	8.1	4.3	3.4	3.5	1.6	5.4	5.7	22.3
Ce	15.5	12.1	11.0	13.4	22.5	12.2	9.8	9.6	4.8	16.4	16.2	49.8
Pr	2.2	1.7	1.6	2.0	3.2	1.7	1.5	1.5	0.72	2.3	2.5	6.3
Nd	11.4	8.8	8.1	9.8	16.4	9.0	7.8	8.1	3.4	11.9	13.3	25.5
Sm	3.5	2.9	2.6	3.0	4.8	2.8	2.6	2.6	1.3	3.7	4.2	5.6
Eu	1.21	1.02	1.08	1.18	1.76	1.05	0.92	0.91	0.51	1.28	1.56	2.02
Gd	4.5	3.7	3.1	3.7	6.6	3.7	3.3	3.5	1.7	4.7	5.8	6.0
Tb	0.82	0.69	0.55	0.65	1.04	0.64	0.62	0.59	0.32	0.86	0.95	0.82
Dy	5.1	4.1	4.4	4.2	7.3	4.3	3.9	3.7	2.1	5.3	6.5	4.9
Ho	1.1	0.92	0.71	0.86	1.5	0.89	0.85	0.81	0.43	1.1	1.4	0.89
Er	3.1	2.5	2.1	2.6	4.6	2.5	2.3	2.2	1.3	3.2	4.1	2.4
Tm	0.43	0.35	0.29	0.36	0.64	0.35	0.33	0.34	0.17	0.44	0.55	0.28
Yb	3.0	2.3	1.9	2.4	4.5	2.5	2.2	2.4	1.2	3.0	3.9	2.0
Lu	0.45	0.35	0.29	0.34	0.55	0.33	0.33	0.36	0.17	0.45	0.54	0.27
Hf	2.8	2.2	1.7	2.1	3.7	2.1	2.1	2.0	1.1	3.0	3.0	4.2
Ta	0.38	0.30	0.25	0.27	0.48	0.24	0.26	0.25	0.16	0.40	0.16	1.8
Pb	0.84	0.40	2.3	0.50	2.3	0.41	0.62	0.69	0.40	0.54	0.25	5.1
Th	0.64	0.39	0.27	0.38	0.62	0.34	0.34	0.34	0.10	0.56	0.22	2.0
U	0.15	0.11	0.08	0.11	0.12	0.08	0.09	0.09	0.04	0.13	0.08	0.69

na = not analyzed; OJP-S = Singgalo Basalt; OJP-K = Kwaimbaita Basalt; Mal. = Malaita; Mak. = Makira. See Tejada et al. (2002) and Van Dyke (2000), for complete data sets.

Table 2
Abundances of the platinum-group elements (ng/g) with 2σ errors in the basalts

Sample	Ir	2σ	Ru	2σ	Rh	2σ	Pt	2σ	Pd	2σ
OJP Singgalo basalts										
SGB-11	**0.19**	0.12	0.74	0.15	**0.11**	0.06	4.45	1.62	1.92	0.29
SGB-15	**1.00**	0.50	0.61	0.20	0.57	0.18	6.97	2.32	6.24	1.16
KF-1	**0.27**	0.12	**0.25**	0.10	*0.16*	0.05	**7.37**	0.82	**2.46**	1.49
KF-32	0.34	0.13	2.21	0.11	**0.95**	0.07	6.41	0.08	21.7	0.1
MATA-7	**0.23**	0.05	0.26	0.08	0.15	0.12	3.77	1.05	1.73	0.86
WHTO-15	**0.41**	0.22	*0.20*	0.09	*0.09*	0.08	5.95	0.93	**1.36**	0.83
OJP Kwaimbaita basalts										
SGB-22	bdl		**0.25**	0.16	**0.13**	0.11	8.39	0.04	10.8	0.3
SGB-25	**0.22**	0.11	**0.75**	0.12	0.22	0.16	**5.86**	0.98	**5.26**	0.45
ML-475	1.33	0.06	1.58	0.83	1.30	0.53	27.3	1.7	45.4	8.7
ML-476	1.11	0.49	**1.06**	0.59	1.00	0.22	19.8	3.1	50.5	9.6
MORB-type basalt										
MATA-3	**0.35**	0.06	**0.35**	0.06	**0.14**	0.04	5.28	0.83	1.56	0.49
OIB-type basalt										
WHTO-36	bdl		**0.33**	0.29	0.42	0.30	9.0	2.5	3.7	2.8
Reference material UMT-1										
Average ($n=14$)	8.47	0.36	10.98	0.43	9.59	0.43	129.8	4.0	102.1	4.6
Certified	8.8	0.6	10.9	1.5	9.5	1.5	129	5	106	3
Reproducibility										
SGB-11 ($n=2$)	0.21	0.18	0.69	0.15	0.17	0.11	4.14	1.54	2.21	1.65
SGB-25 ($n=3$)	0.31	0.09	0.98	0.32	0.45	0.26	6.93	0.49	4.87	0.90

bdl = below detection limit. Italicized values are below the 3σ value of the blank analysis, but are statistically above zero. Values in bold are between 3σ and 10σ of the blank analysis. All other values are >10σ of the blank analysis. Errors are calculated following the method of Ely and Neal (2002).

et al. (1999). Therefore, this method cannot be used to quantify Au in samples with high Ta abundances (i.e., >0.05 μg/g). Furthermore, because we are using a quadrupole ICP-MS with a mass resolution of only 1 amu, isotope dilution is not possible because two interference-free isotopes of the individual PGEs are not available. For better precision, the most abundant isotopes of the PGEs were used unless there was an unavoidable interference (e.g., HfO^+). Therefore, ^{191}Ir, ^{102}Ru, ^{103}Rh, ^{198}Pt, and ^{105}Pd were the isotopes quantified.

Detection limits were calculated for each sample analyzed from a blank analysis just prior to the sample and accounting for the dilution factor of the sample. We have made the distinction between data that lie below 3σ (judged to be essentially below detection), between 3σ and 10σ (i.e., between the detection and quantitation limits) and those data that lie above 10σ of the blank value (Table 2). Note that each blank was analyzed six times and averages and standard deviations were then calculated. Column yield was monitored by the frequent analysis of PGE reference material UMT-1 (CANMET: http://www.nrcan.gc.ca/mms/canmet-mtb/ccrmp/umt-1.htm) so that at least one reference material analysis was run with every two samples. While the PGE abundances of UMT-1 are not at the levels of the basalts, this was the best well-characterized reference material available at the time of this study that had certified values available for each of the PGEs quantified. Reproducibility on the basis of 14 analyses of UMT-1 over the period of analysis is better than 5% (Table 2). On the basis of UMT-1 analyses, column yield was consistently better than 93% for Ir and Pd, and 96% for Ru, Rh and Pt. One basalt, SGB-25, was analyzed three times with all analyses in error of each other, and reproducibility on

this basis was Ir (29%), Ru (33%), Rh (58%), Pt (7%) and Pd (19%) (Table 2).

3. Results

Primitive mantle-normalized PGE plots of the OJP basalts show there is general overlap between the Singgalo and Kwaimbaita groups, regardless of age (Fig. 1; Tables 1 and 2). Several basalts exhibit either a flattening of their primitive mantle-normalized profiles between Pt and Pd or a relative Pd depletion. In addition, several also exhibit a slight increase in the normalized Ir abundance. This is most likely a function of the actual abundance being close to the detection limit (i.e., between 3σ and 10σ of the blank in most cases; see Table 2) that generally produces larger errors (usually greater than 40% at the 2σ level; see Ely and Neal, 2002, for details). It is also possible that it is a function of chromite fractionation, based on the partition coefficients derived by Puchtel and Humayun (2001).

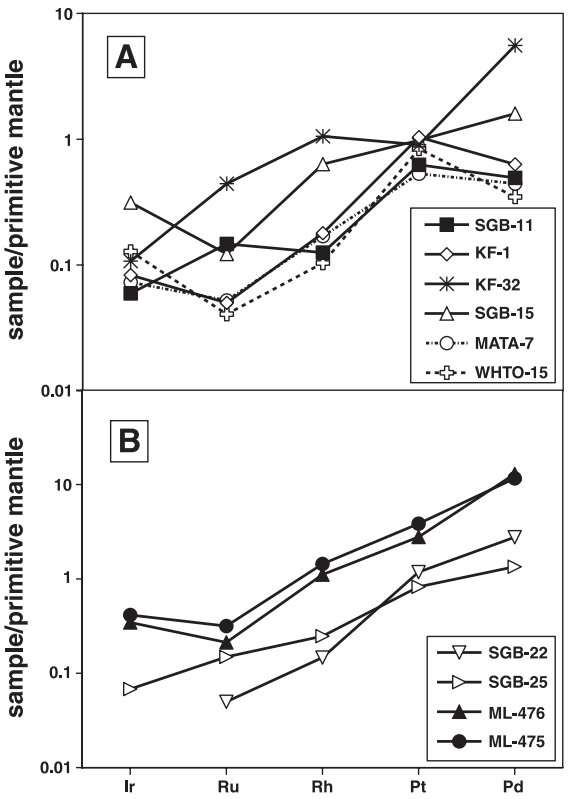

Fig. 1. Primitive mantle-normalized PGE profiles of the OJP basalts analyzed in this study. (A) Singgalo basalts from Malaita and Makira, Solomon Islands; (B) Kwaimbaita basalts from Malaita, which are stratigraphically beneath the Singgalo Formation (Tejada et al., 2002). Note that most of the Singgalo basalts display depletions in Pd relative to Pt (see text for discussion). In addition, several basalts exhibit an enrichment of Ir relative to Ru. This feature is likely an artifact of the larger errors associated with the Ir analyses (see Table 2) or it could possibly be a product of chromite fractionation (see text for discussion). Primitive mantle values are from McDonough and Sun (1995). Two sigma errors are not shown in the figure for simplicity but are given in Table 2 for all the PGE data.

ML-475 and ML-476 deserve special mention because they come from the deepest parts of the plateau exposed on Malaita (Petterson, 1995) and contain the highest PGE abundances of the OJP basalts analyzed in this study (Fig. 1B and Table 2). The major element composition of these two samples, collected consecutively from the Kwaimbaita River on Malaita, Solomon Islands (Petterson, 1995; Tejada et al., 2002), form the extremes of all OJP basalts collected from Malaita (Neal et al., 1997; Tejada et al., 2002). ML-475 is the most Mg-rich (9.99 wt.%), while ML-476 is the least Mg-rich (5.83 wt.%). Note that the MgO content of 86 non-cumulate OJP basalts analyzed from Malaita (Tejada et al., 2002; Neal, unpublished data) have a range of 4.5–8.9 wt.% with an average of 7.35 ± 0.5 wt.% (1σ). Petrography indicates that ML-475 and ML-476 are cumulates. Major element differences reflect modal abundance variations between these two rocks, with ML-475 being dominated by clinopyroxene, resulting in the highest CaO content of any OJP basalt from Malaita (14.5 wt.%) compared to the average of 11.6 ± 0.8 wt.% (1σ). ML-476 contains less clinopyroxene and more titanomagnetite, reflected by the fact that it has the highest TiO_2 [2.07 wt.% compared to the average of 1.47 ± 0.2 wt.% (1σ)] and Fe_2O_3 [18.5 wt.% compared to the average of 13.3 ± 0.7 wt.% (1σ)] contents of any OJP basalt from Malaita (Table 1).

Basalts with trace element compositions similar to MORB (MATA-3) and OIB (WHTO-36) were taken from flows stratigraphically intercalated with the OJP basalts (Van Dyke, 2000). MORB-type sample MATA-3 contains PGE abundances at the upper end of the MORB range (Fig. 2A). OIB-type sample WHTO-36 contains Ru, Rh and Pd abundances that fall within the field defined by Hawai-

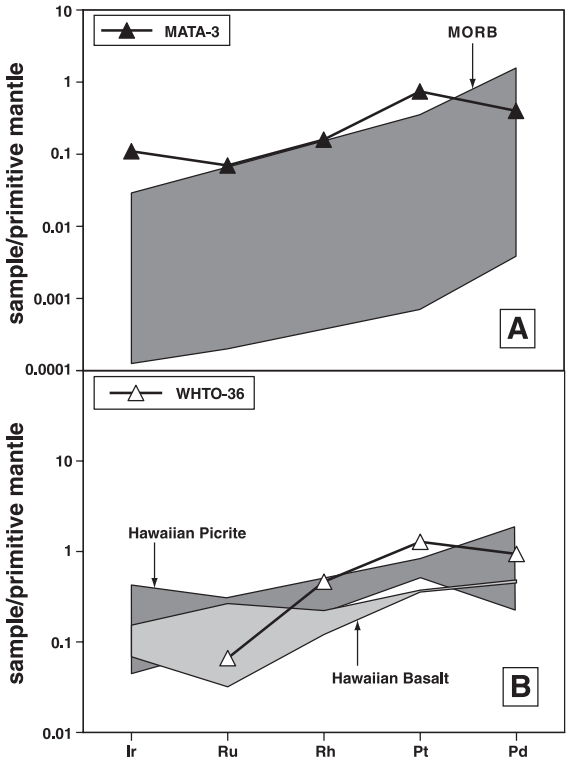

Fig. 2. Primitive mantle-normalized PGE profiles of the MORB-type (A) and OIB-type sample (B). (A) MORB-type basalt MATA-3 just overlaps with a MORB field defined by data from Tatsumi et al. (1999) and Rehkämper et al. (1999). (B) The PGE profile of the OIB-type basalt WHTO-36 appears more fractionated than Hawaiian basalts and picrites (fields from data in Tatsumi et al., 1999 and Bennett et al., 2000). Primitive mantle values are from McDonough and Sun (1995). Two sigma errors are not shown in the figure for simplicity but are given in Table 2 for all the PGE data.

ian basalts and picrites, but contains higher Pt (Fig. 2B).

4. Discussion

4.1. Pd depletions in the OJP basalts

The MORB-type (MATA-3) and OIB-type (WHTO-36) basalts, as well as many of the Singgalo samples exhibit Pd depletions relative to Pt when normalized to primitive mantle abundances. Samples SGB-11 (with Pd depletion) and SGB-25 (with no Pd depletion) were replicated two and three times, respectively, to demonstrate the Pd depletion was not an artifact of a single analysis. Note that none of the Kwaimbaita basalts, coming from deeper within the OJP sequence, exhibit such depletions. As profiles with no Pd anomaly were produced, it is unlikely that this is an artifact of the cation exchange procedure. Several possibilities exist for the apparent preferential fractionation of Pd from the rest of the PGEs, including chromite fractionation/accumulation, sulfide immiscibility and weathering. Palladium is likely to be relatively incompatible in chromites based on the spinel/basalt liquid experimental partition coefficient ($D < 0.02$; Capobianco et al., 1990, 1994) and measured partition coefficients from komatiites ($D \sim 1.6$, the lowest value of the PGEs; Puchtel and Humayun, 2001). Furthermore, Pd abundances in chromitites are low compared to other PGEs (e.g., Prichard and Lord, 1990a). However, it is not evident that chromite is the controlling factor on Pd abundances, as it would have been a much earlier crystallizing phase and there is no correlation of $[Pt/Pd]_{PM}$ with $[Cr/Cu]_{PM}$ (Fig. 3) or between Pd and Cr abundances.

The positive correlation of Pt and Pd abundances in mantle-derived magmas (Fig. 4) demonstrates the coherent behavior of these elements during partial melting and subsequent modification as the magma cools. The wide range in komatiite and komatiitic basalt PGE abundances is a result of enrichment/depletion by sulfide addition/extraction that has dramatically increased Pt and Pd abundances in certain komatiites from northern Ontario (Fig. 4; Barnes and Naldrett, 1986). Note that the OJP data, for the most part, form a vertical trend generated by the variation in Pd (Table 2). Sulfide liquid/silicate melt partitioning experiments show a range of values, depending upon experimental conditions, for both Pt (900–46,000) and Pd (1800–140,000) (see Walter et al., 2000 for review as well as Fleet et al., 1999). Generally, the partition coefficient for Pd is 1.5–2 times that of Pt. Therefore, extraction of a sulfide liquid may cause a relative depletion in Pd. However, the magnitude of the sulfide liquid/silicate melt partition coefficients would mean that the overall abundances of all the PGEs in our samples would be <1 ng/g and similar to abundances in many MORB samples (see next section).

Several studies of ore deposits have found Pd to be more mobile than Pt in surficial environments, often being transported away in solution (e.g., Wood and Vlassopoulos, 1990). This is apparently independent

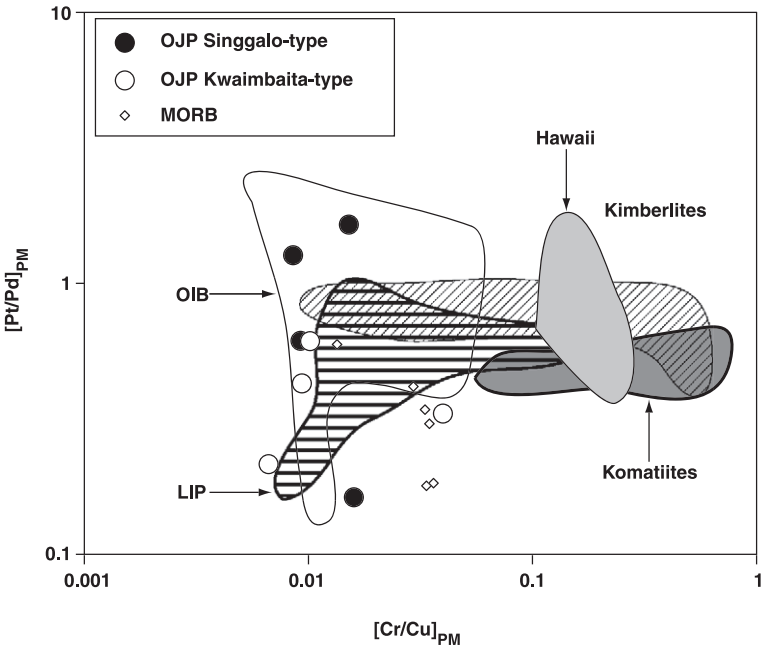

Fig. 3. Plot of $[Pt/Pd]_{PM}$ vs. $[Cr/Cu]_{PM}$ ratios of OJP basalts from Malaita compared with komatiites, kimberlites, Hawaiian basalts and picrites, LIP basalts, and OIB fields as well as MORBs. The subscript "PM" represents the ratio normalized to primitive mantle abundances. The OJP samples form a general horizontal trend, consistent with removal of Pd by weathering. Komatiite data are from Arndt and Nesbitt (1984), Arndt (1986), Brügmann et al. (1987, 1993), Puchtel et al. (1996), and Puchtel and Humayun (2001) and references therein. OIB data are from Greenough and Fryer (1990), Fryer and Greenough (1992), Rehkämper et al. (1999) and references therein. The LIP field is defined by the Noril'sk basalt data of Lightfoot et al. (1990) and Brügmann et al. (1993) and references therein, and Iceland tholeiite data from Hemond et al. (1993) and Rehkämper et al. (1999). Hawaii data are from Tatsumi et al. (1999), Norman and Garcia (1999), and Bennett et al. (2000). MORB data is from Tatsumi et al. (1999) and Rehkämper et al. (1999) and references therein. Kimberlite data are from McDonald et al. (1995). Primitive mantle values are from McDonough and Sun (1995).

of climate (e.g., Brazil—Taufen and Marchetto, 1989; Madagascar—Salpeteur and Jezequel, 1992; Canada—Wood and Vlassopoulos, 1990; Shetland Islands, UK—Prichard and Lord, 1990b). Such behavior has also been quantified in experimental studies (Wood, 1990; Bowles et al., 1994). Furthermore, Barnes et al. (1985) concluded that hydrothermal alteration preferentially mobilized Pd. Petrographic observations of the OJP basalts show variable alteration of the primary phases to secondary minerals, especially of the glass and mesostasis, as well as the rare olivine phenocrysts (see Samples and analytical methods). The OJP basalts were emplaced in a submarine environment as pillow basalts, thus, there are significant joint systems for chloride-rich hydrothermal fluids to move through the basalts, which could facilitate the preferential mobilization of Pd (e.g., Mountain and Wood, 1988). This is evident from the high Cl/K ratios in the OJP basalts, which indicate some shallow-level assimilation of hydrothermally altered crust (Michael and Cornell, 1996; Michael, 1999). Although the freshest samples possible were taken (i.e., from the pillow interiors), it is possible that even these have experienced submarine and subaerial tropical weathering processes, which could be the mechanisms for generating the observed Pd depletions. Variation in $[Pt/Pd]_{PM}$ and $[Cr/Cu]_{PM}$ ratios illustrate this (Fig. 3), showing that the OJP basalts dated at 122 Ma generally follow a vertical trend indicative of weathering. The Kwaimbaita samples do not exhibit Pd depletions and are from deeper within the OJP section and therefore were rapidly buried by subsequent eruptions, resulting in relatively less alteration. The Singgalo basalts were the last OJP eruptive event recorded on Malaita and therefore were subjected to low-temperature alteration processes for a

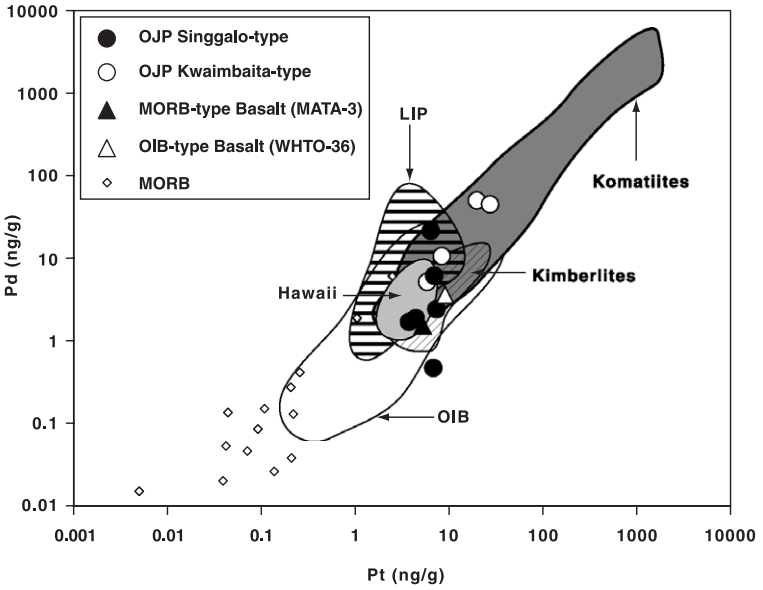

Fig. 4. Covariation of Pt and Pd in samples analyzed in this study compared to other mantle-derived magmas. The Singgalo basalt data stand out because they form a vertical trend on this diagram, which is interpreted as being consistent with preferential mobilization of Pd during low temperature alteration (see text for discussion). Data sources for the fields and MORBs are as in Fig. 3, with the addition of komatiite data from Barnes and Naldrett (1986), Crocket and MacRae (1986), and Barnes and Picard (1993).

long period of time. We believe that the Pd depletions are therefore a low-temperature alteration effect.

4.2. PGE fractionation processes

Fractionated PGE profiles can be generated during partial melting of mantle peridotites, as Ir (and presumably Os) is the most compatible (bulk partition coefficient >6) and the PGEs showing decreasing compatibility to Pd (bulk partition coefficient ~ 0.2) (Barnes and Picard, 1993). Although Burton et al. (2002) suggested Os (and by inference Ir) is *incompatible* in olivine, positive correlations of Ir with MgO have been reported for terrestrial basalts (e.g., Righter et al., 2000) and Os with MgO for Hawaiian basalts (Hauri et al., 1996). The general correlation of Ir with magnesium number and Cr (cf. Barnes and Picard, 1993; Righter et al., 2000) suggests Ir and presumably Os are compatible in olivine and/or chromite (Barnes et al., 1985; Handler and Bennett, 1999; McCandless et al., 1999), and detailed analyses of mineral separates generally support this (e.g., Brügmann et al., 1987; Zhou et al., 1998; Vatin-Perignon et al., 2000; Puchtel and Humayun, 2001). While the theory that small sulfide inclusions in these separates may elevate PGE contents cannot be entirely discounted, it is generally recognized that high-Mg lavas contain high PGE contents (cf. Brandon et al., 1999; Righter et al., 2000). As the OJP basalts are not primary magmas (e.g., Mahoney et al., 1993; Neal et al., 1997), fractional crystallization may also have affected the overall PGE abundances. This is seen in ML-475 and ML-476, which contain the highest PGE abundances of all analyzed OJP basalts (e.g., Figs. 4 and 5) and exhibit textural and geochemical evidence of crystal accumulation; accumulation of fractionated phases in these samples has preserved the general fractionated PGE profile seen in the OJP basalts, but has elevated the PGE abundances.

The presence of sulfide phases can also radically affect PGE abundances in mafic melts. Processes involving varying degrees of sulfide removal or incorporation have been invoked to account for the PGE contents of ocean island basalts formed at much lower degrees of partial melting than the OJP basalts (Handler and Bennett, 1999; Bennett et al., 2000). Sun (1982) gave lower and upper estimates for the amount of sulfide in the mantle of 0.1% and 0.3%, respec-

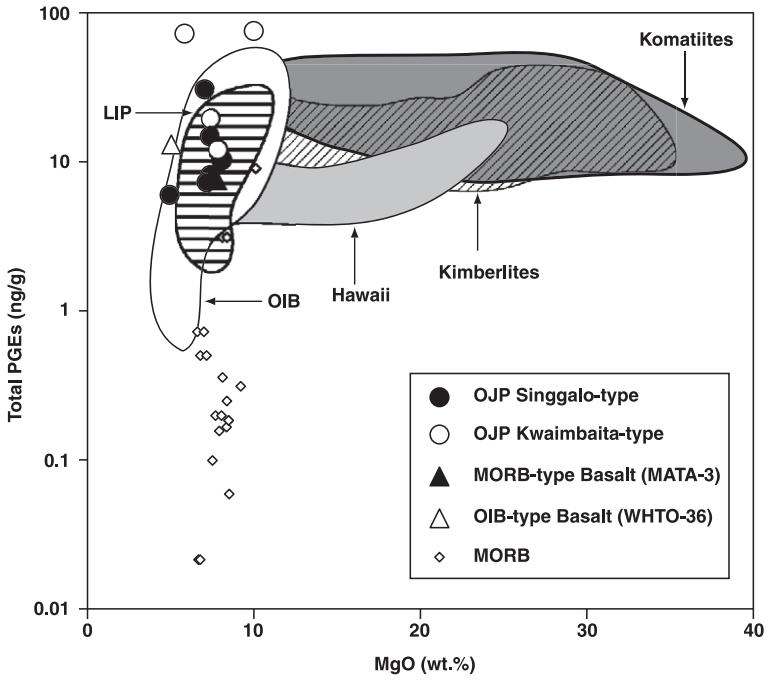

Fig. 5. Comparisons of variations in total PGEs (ng/g) with MgO (wt.%) of samples analyzed in this study with other mantle-derived magmas. The total PGE content was calculated by summing Ir, Ru, Pt and Pd abundances. Rh was omitted because literature values for this element are not abundant. Data sources for the fields and MORBs are the same as in Figs. 3 and 4.

tively. Assuming a maximum sulfur solubility in magma of 0.26% (Wendlandt, 1982), the lower and upper sulfide estimates will be exhausted at 13% and 38% partial melting. Barnes et al. (1985) used an estimate of 25% partial melting to exhaust all sulfide in a mantle source, whereas Fryer and Greenough (1992) estimated 23% partial melting was required. Bulk mantle S contents are estimated at 200–250 μg/g (McDonough and Sun, 1995; Holzheid and Grove, 2002), which corresponds to a modal sulfide abundance of $<0.1\%$, so the amount of partial melting required to exhaust it may be lower than even the 23% used by Fryer and Greenough (1992). In the case of the OJP basalts, estimates of partial melting from rare earth element inversion techniques (cf. McKenzie and O'Nions, 1991) suggested degrees of partial melting were $\sim 30\%$ (Mahoney et al., 1993), more than required to exhaust sulfide in a mantle source, thus negating fractionation into a sulfide-bearing residuum. The fact that the PGE primitive mantle-normalized patterns of all OJP basalts, except Pt and Pd in ML-475 and ML-476, are within error of each other suggests large degrees of partial melting may have homogenized PGE contents no matter what isotopic group the basalts are from or age at which they were erupted. The relatively high PGE abundances in the MORB-type and OIB-type samples would again suggest no residual sulfide remained in the source regions of these magmas after partial melting.

Barnes and Picard (1993) concluded that extraction of a small amount of immiscible sulfide liquid or a sulfide phase preferentially controlled Rh, Pt and Pd abundances in their study of Proterozoic basalts. This explained the lack of correlation between these PGEs and incompatible lithophile elements in their study. The lack of appreciable sulfide in thin sections of our samples suggests either an immiscible sulfide phase may have been removed during the evolution of the magmas or the evolution paths did not reach sulfide immiscibility. Michael and Cornell (1996) noted that OJP basalts are undersaturated with respect to sulfur. This may have been caused by sulfide immiscibility, as the sulfide-rich liquid could have separated on the ascent of the magma or segregated at lower depths

because of its higher density (Barnes and Picard, 1993). As the sulfide melt/silicate melt partition coefficient for Cu is approximately half that of Pt (e.g., Fleet and Stone, 1991), segregation of sulfide could explain the fact that for the majority of samples, $[Cu/Pt]_{PM} \neq 1$ (Fig. 6). However, the OJP basalts have experienced relatively large degrees of crystal fractionation (e.g., Mahoney et al., 1993; Neal et al., 1997) that may have increased $[Ti/Pt]_{PM}$ and $[Cu/Pt]_{PM}$ ratios, especially as Cu, Ti and Pt are incompatible in olivine, while Cu and Ti are incompatible in chromite, but Pt is moderately compatible in chromite (Puchtel and Humayun, 2001). Note that ML-475, a clinopyroxene cumulate, contains lower $[Cu/Pt]_{PM}$ and $[Ti/Pt]_{PM}$ ratios, suggesting that Pt is more compatible in clinopyroxene than Cu or Ti. The MORB-type and OIB-type samples plot below the komatiite, LIP, OIB and MORB fields, having higher $[Ti/Pt]_{PM}$ ratios for a given value of $[Cu/Pt]_{PM}$. Such a relationship could be facilitated by extraction of an immiscible sulfide liquid from an evolving LIP magma, but isotopic and trace element evidence argues for separate sources for these magmas (cf. Van Dyke, 2000; Tejada et al., 2002).

Evidence that the OJP basalts have not experienced extraction of an immiscible sulfide phase can be seen from plotting ratios of lithophile to chalcophile elements (e.g., $[Y/Cu]_{PM}$) against ratios of PGE to lithophile elements (e.g., $[Pt/Y]_{PM}$) (Fig. 7). As noted by Neal et al. (1997), the dominant crystallizing phases in the evolution of the OJP basalts were olivine, a spinel phase, clinopyroxene and plagioclase. Fractionation of these phases would produce a decrease in the $[Pt/Y]_{PM}$ ratio (Pt is slightly compatible and Y is incompatible) with little change in the $[Y/Cu]_{PM}$ ratio (both are broadly incompatible). Removal of a sulfide phase from a basaltic magma would result in a major increase of $[Y/Cu]_{PM}$ and a decrease in $[Pt/Y]_{PM}$. For example, the lobe in the LIP field towards higher $[Y/Cu]_{PM}$ and lower $[Pt/Y]_{PM}$ is defined by basalts from Noril'sk that have experienced the extraction of an immiscible sulfide melt (cf. Brügmann et al., 1993). The MORB-type basalt has an elevated $[Y/Cu]_{PM}$ suggestive of sulfide removal, but the PGE abundances are relatively high for MORBs; the normalized PGE profile parallels the most enriched Pacific MORB sample that apparently has not experienced sulfide immiscibility (Fig. 2A).

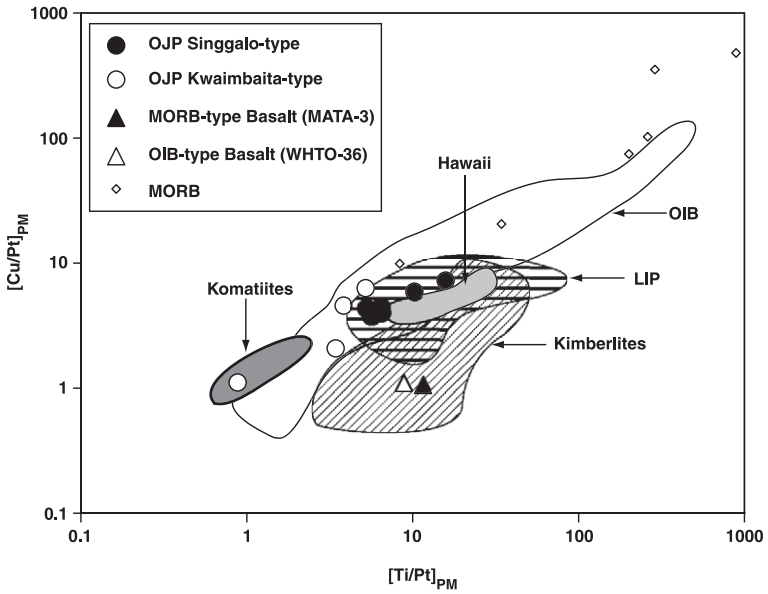

Fig. 6. Plot of $[Cu/Pt]_{PM}$ vs. $[Ti/Pt]_{PM}$ ratios from samples analyzed in this study compared to other mantle-derived magmas. Note that ML-475 (a basalt that has accumulated clinopyroxene) plots in the komatiite field. The OIB-type basalt from Makira plots outside the OIB field and the MORB-type basalt from Makira plot away from other MORB data. Data sources for the fields and MORB are as in Figs. 3 and 4, except there is no comparison to East Pacific Rise (EPR) MORB due to lack of Cu data in the literature. The MORB data are supplemented by data from Devey et al. (1994) and Hemond et al. (1993). Primitive mantle values are from McDonough and Sun (1995).

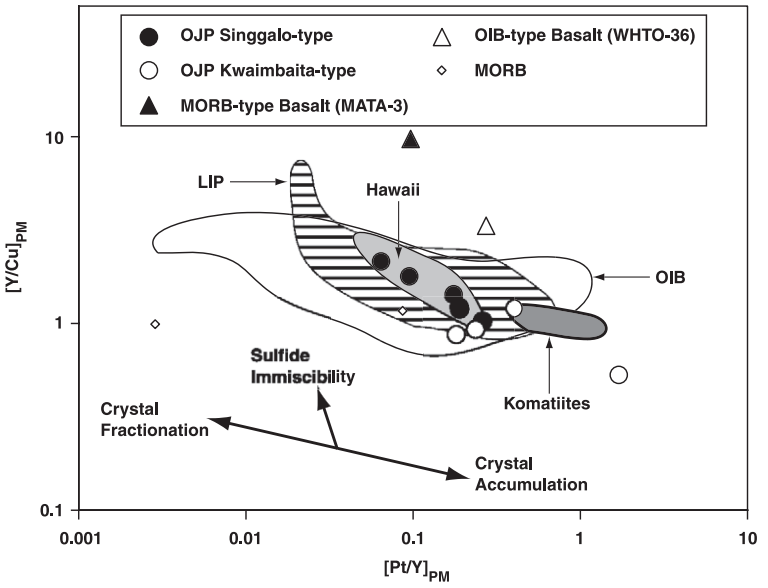

Fig. 7. Plot of $[Y/Cu]_{PM}$ vs. $[Pt/Y]_{PM}$ ratios of OJP basalts and MORB-type and OIB-type basalts from Makira with other mantle-derived magmas. Note that ML-475 plots beyond the komatiite field and the OJP sample data form a trend consistent with crystal fractionation/accumulation. The sub-vertical limb of the LIP field is defined by basalts from Noril'sk that have experienced extraction of an immiscible sulfide liquid (Brügmann et al., 1993). Data sources for the fields and MORBs are as in (Figs. 3, 4 and 6). Primitive mantle values are from McDonough and Sun (1995).

While Fig. 7 can be a useful indicator for the effect of sulfide removal on an evolving basaltic melt, we note that Cu can be mobile during hydrothermal alteration (e.g., Alt et al., 1986) and this may produce anomalously high $[Y/Cu]_{PM}$ ratios. Therefore, to fully evaluate a basaltic sample for the effects of sulfide, other geochemical parameters must be considered. As noted above, the PGE abundances in our samples are consistent with the parental magmas not experiencing sulfide removal and apart from MORB-type basalt, MATA-3, all our samples plot along the fractional crystallization trend in Fig. 7. Therefore, for the samples studied here, we conclude that sulfide removal/retention has not been a factor in their evolution.

4.3. Source of PGEs in OJP magma

The OJP basalts possess similar PGE contents to Hawaiian picrites (Bennett et al., 2000) and kimberlites (McDonald et al., 1995) (Fig. 4). Unlike the OJP basalts, these were formed by relatively low degrees of partial melting and possibly retained sulfide in the source to varying degrees (Bennett et al., 2000). However, the OJP basalts are strongly fractionated relative to the Hawaiian picrites and kimberlites (Fig. 5). Using the crystal fractionation scheme similar to that proposed by Neal et al. (1997) for the OJP basalts (see Section 4.4.2 below for details) in conjunction with the partition coefficients listed in Table 3, the bulk K_d is >1 for all of the PGEs except Pd. This implies that the primary magma(s) for the OJP basalts contained higher PGE abundances. Note also that cumulate samples ML-475 and ML-476 contain elevated PGE contents (Fig. 5). Furthermore, while they plot between the OIB + LIP fields and the sulfide-enriched komatiites in Fig. 4, there is no petrographic or geochemical evidence for sulfide enrichment in these samples. Therefore, relative to other mantle-derived magmas, the OJP basalts, including the MORB-type and OIB-type samples, were derived at various times since the surfacing of the OJP plume head at ~ 122 Ma from sources relatively enriched in the PGEs.

The OIB-type sample (WHTO-36) has a more fractionated primitive mantle-normalized PGE pattern than the OJP basalts (Fig. 2B; Pt/Ru for WHTO-36 is

Table 3
Modeling parameters

	Ir	Ru	Rh	Pt	Pd	Reference
Partition coefficients						
Olivine	0.77	1.7	1.8	0.08	0.03	1
Clinopyroxene	*1.8*	1.9	3.0	2.2	0.3	2
Chromite	100	152	*50*	3.3	1.6	3
Orthopyroxene	*1.8*	1.9	3.0	2.2	0.3	*
Plagioclase	*0.3*	0.3	0.4	*0.3*	0.2	4
Magnetite	*500*	300	130	*3*	1.1	5
Sulfide	4400	2400	*3000*	6900	6300	6
Metal	1.66×10^6	2.8×10^6	3.9×10^6	5.1×10^6	6.2×10^6	7
Components						
Outer Core	188	669	134	776	572	8
Lower (primitive)						
Mantle	3.2	5.0	0.9	7.1	3.9	9
Upper Mantle	2.46	4.29	*1.0*	4.34	2.48	10
Depleted upper						
Mantle	2.67	4.69	1.08	4.29	1.67	11

1 = Malvin et al. (1986), Puchtel and Humayun (2001), Capobianco et al. (1994), Capobianco and Drake (1994); 2 = Malvin et al. (1986), Capobianco and Drake (1994), Righter (1999); 3 = Puchtel and Humayun (2001); 4 = Capobianco et al. (1994); 5 = Capobianco et al. (1991, 1994); 6 = Fleet et al. (1991, 1994), Bezmen et al. (1994), Tredoux et al. (1995); 7 = Jones and Drake (1986), Borisov et al. (1994); 8 = Snow and Schmidt (1998); 9 = McDonough and Sun (1995); 10 = Rehkämper et al. (1997); 11 = calculated in this study; * = orthopyroxene partition coefficients assumed to be the same as for clinopyroxene. Italicized values are estimated.

27.5 vs. 9.2 for the average OJP basalt). The MORB-type basalt has lower PGE abundances than the OIB-type sample and plots at the upper end of MORB compositions in Fig. 2A, but higher than published data for East Pacific Rise (EPR) MORB (Tatsumi et al., 1999). Being stratigraphically intercalated with the OJP basalts on Makira, it is conceivable that the Makira MORB-type basalt could have been contaminated by OJP components, although where this contamination occurred is equivocal. This is evident from $[Nb/Zr]_{PM}$ and $[Pt/Y]_{PM}$ ratios (Fig. 8), which shows that the OJP basalts plot in between the OIB-type sample from Makira and MORB, with the MORB-type basalt from Makira containing a similar $[Nb/Zr]_{PM}$ ratio to MORB, but has elevated $[Pt/Y]_{PM}$ similar to the OJP basalts. The $[Nb/Zr]_{PM}$ spread in the OJP basalt data from Malaita is consistent with crystal fractionation and clinopyroxene ± titanomagnetite accumulation (note the location of ML-475 in Fig. 8). The crystal fractionation scheme [defined in Neal et al. (1997)—see Section 4.4.2 below for details], in conjunction with the partition coefficients in Table 3, would produce a range of $[Pt/Y]_{PM}$ ratios but only minor changes in $[Nb/Zr]_{PM}$. While the samples plotted in Fig. 8 represent different ages of OJP volcanism, it clearly demonstrates that Singgalo and Kwaimbaita basalt source regions were long-lived. As the magnitude of OJP magmatism waned, it is possible that the well-mixed nature of the source regions began to break down so that MORB-type and OIB-type magmas were erupted and intercalated in the LIP stratigraphy. The presence of a distinct mantle "root" beneath and attached to the OJP, interpreted to be the remnants of the initial OJP plume head (Richardson et al., 2000), suggests a plume source was added to the upper mantle at ~ 122 Ma that could be subsequently retapped, producing more recent OJP-type volcanism as observed on Santa Isabel (Tejada et al., 1996) and Makira (Van Dyke, 2000). According to the model of Richards et al. (1989) and Campbell and Griffiths (1990), magmas derived from the plume head would be distinct to those derived from the plume tail, with the latter being "OIB-like" in their geochemistry. While the intercalated OIB-type basalts are rare in the OJP basalt sequence, they may represent evidence of the OJP

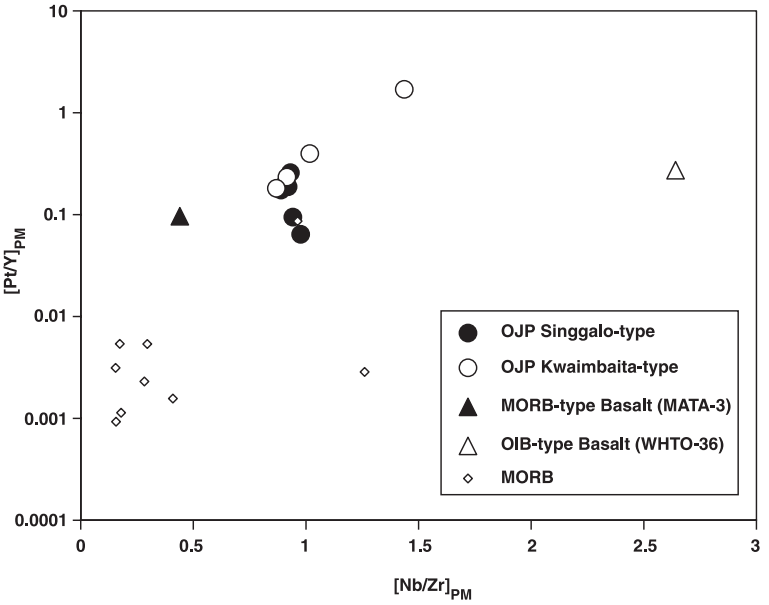

Fig. 8. Variations in $[Pt/Y]_{PM}$ and $[Nb/Zr]_{PM}$ ratios from samples analyzed in this study and MORBs. The effects of crystal fractionation/accumulation would form a near vertical trend on this plot, as defined by the OJP basalt data. Data sources for MORBs are the same as in (Figs. 3, 4 and 6). Primitive mantle values are from McDonough and Sun (1995).

plume tail (Van Dyke, 2000). Our OIB-type sample (WHTO-36) forms an end-member source composition in Fig. 8. Furthermore, partial melting of 5% would alter the $[Nb/Zr]_{PM}$ ratio by ~ 1 unit (see Neal et al., 1997 for further details), which is not enough to generate our OIB-type sample from an OJP basalt source. The MORB-type sample, MATA-3, may therefore represent a component of depleted upper mantle that has been entrained in the OJP plume head and at ~ 44 Ma has subsequently been remobilized. Based on both the $[Pt/Y]_{PM}$ and $[Nb/Zr]_{PM}$ ratios, it is a reasonable conclusion that MATA-3 has been contaminated with OJP melts or components.

4.4. Partial melting and fractional crystallization modeling

We have produced models in order to investigate the PGE compositions of the OJP and related basalts by illustrating the patterns and PGE abundances produced from known mantle sources. This illustrative modeling is constrained by partial melting and fractional crystallization parameters derived for the OJP from previous modeling efforts (Mahoney et al., 1993; Tejada et al., 1996, 2002; Neal et al., 1997). The modeling has been conducted only using a spinel peridotite source and assumes that whatever the ultimate depth of origin, diapiric upwelling transported the source into the spinel stability field where partial melting occurred. Other possible mantle sources include one composed of garnet peridotite or a garnet peridotite/spinel peridotite hybrid (cf. Neal et al., 1997). There are no literature values for partition coefficients of the PGEs in garnet or majorite, so it was not possible to quantitatively constrain basalt PGE compositions generated from a source region containing these phases. However, although Re may be compatible in garnet (Righter and Hauri, 1998), Mitchell and Keays (1981) ranked garnet last in PGE compatibility of common mantle minerals based on PGE abundances in mineral separates of mantle xenoliths.

The majority of PGE partition coefficients used in our modeling are taken, where possible, from published literature values (see Table 3). The relatively coherent behavior of PGEs as a group allowed us to estimate K_d values for some elements (e.g., Ir in clinopyroxene). As no PGE partition coefficients have been published for orthopyroxene, for the purposes of

this work, they are taken to be the same as those of clinopyroxene. In addition, the modal mineralogy of the spinel peridotite source is taken as the average mode of spinel lherzolite xenoliths from alnöite occurrences on Malaita, Solomon Islands (Neal, 1986). Where necessary, the proportion of olivine is adjusted to account for 0.06% sulfide (estimated from a bulk mantle S value of 200–250 μg/g; McDonough and Sun, 1995; Holzheid and Grove, 2002) and up to 1% metal. In all cases where sulfide was used in the modeling, it was exhausted in the source during partial melting. Finally, our models generally produce Pd abundances that are higher than observed. We attribute this to preferential Pd removal during alteration such that the measured abundance is now lower than the original whole-rock value imparted from magmatic processes (see above).

4.4.1. Upper mantle PGE source for MORB

Using an average spinel peridotite composition from Rehkämper et al. (1997) for the initial PGE abundances (excluding Rh, which was not given and was estimated from the other PGEs provided such that the primitive mantle-normalized pattern was flat from Ru to Pt) and an estimate of 10% partial melting for N-MORB, a non-modal partial melting model was used to model the PGE abundances of the MORB-type basalt, MATA-3. A three-stage Rayleigh fractional crystallization model was applied to the derived melt composition (see Fig. 9). Each stage crystallized 5% of the total magma and the removal of sulfide mimics the immiscibility observed in MORB (e.g., Roy-Barman et al., 1998). Note that while Ir and Ru abundances of MATA-3 are generally within error of those of the OJP basalts, Rh and Pt are lower and outside the 2σ error (Table 2). The N-MORB model generally reproduces the EPR MORB pattern (Fig. 9A), but these modeled PGE abundances are well below OJP basalt abundances and those of MATA-3. However, the PGE profile after the initial crystal fractionation stage mimics the profile for MATA-3, even the slight increase in normalized Ir abundance relative to Ru (Fig. 9A). This feature is caused by the Ir and Ru partition coefficients of Puchtel and Humayun (2001) for chromite (see Table 3). The modeled PGE profiles are changed little using a hybrid source (80% upper mantle, 20% lower or primitive mantle; Fig. 9B) as suggested by Fig. 8. Our modeling reinforces the conclusion that MORB-

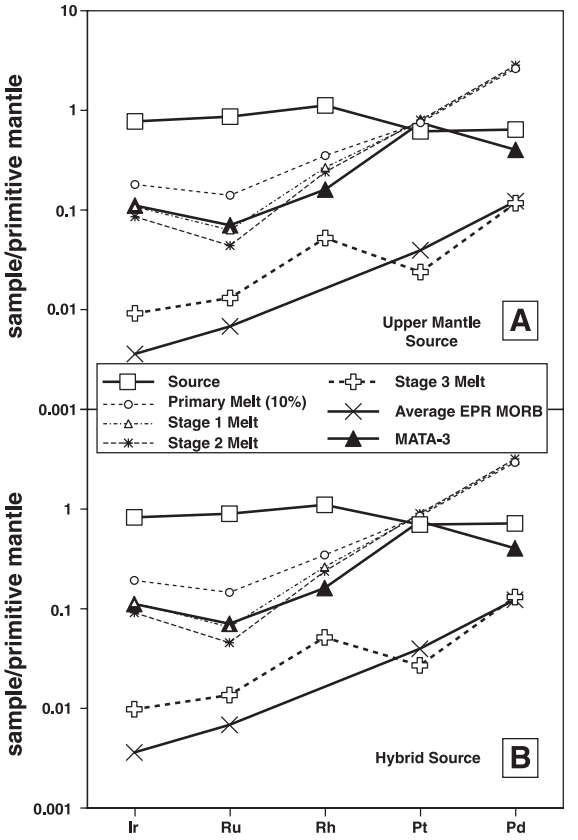

Fig. 9. Model of the primitive mantle-normalized PGE pattern from MORB-type basalt MATA-3 illustrates that this sample has not experienced sulfide immiscibility. Modeling uses a 100% upper mantle source (i.e., spinel peridotite) in (A) and a hybrid source in (B) that is taken as 80% upper mantle and 20% lower mantle (see Table 3 for PGE concentrations). The source composition in each case (Table 3) is a spinel peridotite consisting of 64.94% olivine, 18% clinopyroxene, 4% spinel, 13% orthopyroxene and 0.06% sulfide, melting in the proportions 24:30:20:25.4:0.6, respectively. A three-stage fractional crystallization sequence was applied to the primary melt generated by 10% partial melting that is consistent with known sequences for N-MORB based on petrography and modal abundances (e.g., Bender et al., 1978; Walker et al., 1979; Bryan, 1983): Stage 1 = 90% olivine + 10% spinel; Stage 2 = 15% olivine + 80% plagioclase + 5% spinel; Stage 3 = 10% olivine + 10% clinopyroxene + 79% plagioclase + 1% sulfide. Each stage crystallized 5% of the magma. Note that the MATA-3 PGE abundances and profile is generated after either Stage 1 or Stage 2 of the fractional crystallization sequence. The average EPR MORB requires sulfide extraction, with the apparent Pt anomaly being a function of the sulfide K_ds that were used (see Table 3). Primitive mantle values are from McDonough and Sun (1995).

type basalt MATA-3 has not experienced sulfide fractionation.

4.4.2. Upper mantle PGE source for the OJP basalts

Using the spinel peridotite residue after the extraction of N-MORB as an upper mantle source, modeling was conducted to see if the PGE abundances of the OJP basalts could be generated from it. Non-modal batch partial melting with a minimum degree of partial melting of 10% and a maximum of 30% was used, based on estimates from Mahoney and Spencer (1991), Michael and Cornell (1996) and Tejada et al. (2002). From major and trace element modeling, Neal et al. (1997) proposed that the OJP magma went through five stages of fractional crystallization, which were: Stage 1 = 100% olivine; Stage 2 = 70% olivine + 30% spinel; Stage 3 = 50% olivine + 50% clinopyroxene; Stage 4 = 95% clinopyroxene + 5% plagioclase; Stage 5 = 90% clinopyroxene + 5% plagioclase + 5% orthopyroxene. Each stage crystallized 10% of the original magma volume. We have slightly modified Stages 2 and 5 for the modeling presented here. Stage 2 is now 95% olivine and 5% spinel because 30% spinel fractionation (using the K_ds of Puchtel and Humyan, 2001) causes dramatic depletions in Ir, Ru and Rh, much lower than observed. Stage 5 is now 89.5% clinopyroxene, 5% plagioclase, 5% orthopyroxene and 0.5% titanomagnetite because of petrographic observations from ML-475 and ML-476. In revisiting the modeling presented by Neal et al. (1997), these changes have little effect on the overall outcome of the major and trace element evolution. The primary melts generated from our models are not as fractionated as the OJP basalt profile, but once fractional crystallization of the primary melt has been modeled, the PGE profiles are subparallel to those from basalts with the lowest PGE abundances (Fig. 10A). PGE abundances (except for Pd) are reduced below the OJP field if the degree of partial melting is lowered because Ir, Ru, Rh and Pt are all compatible elements (see Table 3). Our modeling therefore illustrates that the range of PGE compositions recorded by the OJP basalts were not generated solely from an N-MORB-depleted (upper mantle) spinel peridotite source.

4.4.3. Lower mantle PGE source for the OJP basalts

As noted above, it is assumed that *melting* of the OJP source occurred in the spinel peridotite stability field or at the garnet–spinel transition after diapiric rise of the plume head (Neal et al., 1997). A spinel peridotite source with primitive mantle PGE abundances is used to investigate the generation of the OJP basalts from an assumed lower mantle source. Minimum and maximum degrees of partial melting are 10% and 30%, respectively, and the same fractional crystallization sequence was used as described in the previous section. This model results in a more fractionated PGE profile (Pt/Ru ~ 23 vs. 9.2 for the average OJP basalt), although the model produces Ir, Ru and Rh abundances that are similar to the profile of the lowest abundance OJP basalt (Fig. 10B). This modeling is consistent with at least some of the OJP basalts being derived from a primitive (lower) mantle source, but indicates that a source enriched in PGEs *above* primitive mantle abundances is required to generate the complete observed range.

Possible terrestrial sources enriched in PGEs above primitive mantle abundances are the core or a sulfide-rich area of the mantle. However, it is unlikely that a sulfide-rich area in the mantle could be the source of the PGEs in the OJP basalts because the OJP basalts are undersaturated with respect to sulfur, have relatively low sulfur abundances (Michael and Cornell, 1996) and have not experienced sulfide immiscibility (see above). Komatiites (which have similar degrees of partial melting to the OJP basalts) that have lower PGE abundances relative to the OJP basalts still have much higher S abundances than the OJP basalts (e.g., Brügmann et al., 1987, 1993).

Suprachondritic $^{186}Os/^{188}Os$ ratios have been used to suggest the presence of an outer core component in plume-derived picrites and komatiites, caused by the fractionation of the Pt/Os ratio during the crystallization of the inner core and subsequent decay of ^{190}Pt to ^{186}Os (e.g., Walker et al., 1995, 1997; Brandon et al., 1998, 1999). The fractionated nature of the OJP basalts, however, negates Pt–Os isotope determinations to investigate a core signature (as used by Walker et al., 1995, 1997; Brandon et al., 1998, 1999) because Os is removed during crystal fractionation, resulting in a ^{186}Os beam that is insufficient for isotopic analyses of the requisite precision. Parkinson et al. (2001) reported Re–Os abundances and $^{187}Os/^{188}Os$ isotopic data from OJP lavas obtained from Ocean Drilling Program Leg 192. They interpreted their data to show no evidence of a core component in the samples

analyzed; the Re–Os systematics were consistent with a lower mantle source. We have demonstrated above that the PGE contents of at least some of the OJP basalts can be modeled without the need of an outer core component, consistent with the conclusions of Parkinson et al. (2001). Indeed, Brandon et al. (1998, 1999) demonstrated that the core component, hypothesized on the basis of suprachondritic $^{187}Os/^{188}Os$ and $^{186}Os/^{188}Os$ ratios, was not present in every Hawaiian picrite they analyzed. However, on the basis of our PGE model, those OJP basalts with relatively high PGE abundances cannot be generated solely by a lower mantle source.

Several recent geophysical studies have provided evidence of at least localized mixing between the outer core and the lower mantle (Vinnik et al., 1998; Wen and Helmberger, 1998; de Wijs et al., 1998). Geodynamic and geophysical modeling predict the formation of the OJP plume at the CMB (e.g., Coffin and Eldholm, 1993), which suggests that it is feasible for the enriched PGE contents of at least some of the OJP basalts to be modeled using entrained outer core material. The effect on major element contents would be minimal and difficult to see. Assuming the core is >90% Fe, adding <1 wt.% of this material to and exhausting it from the source would change the iron content by <1 wt.%. Furthermore, the effect would be further diluted by fractional crystallization to the point where it would be impossible to detect any spurious Fe addition to the basalt source.

We have conducted modeling to illustrate the effects that inclusion of an outer core component in the

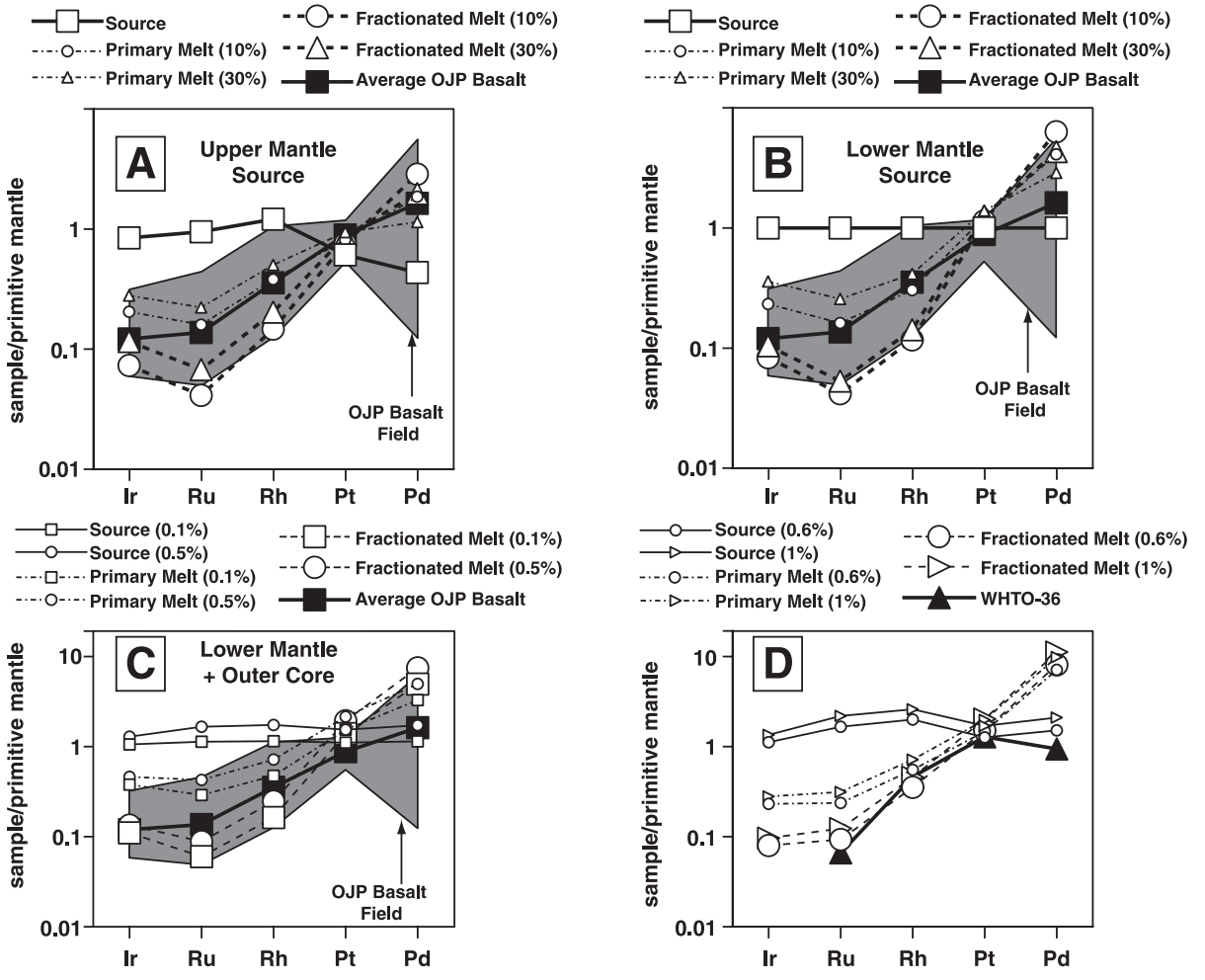

source of the OJP basalts has on the PGE contents. The PGE composition of the outer core component used in our modeling was that proposed by Snow and Schmidt (1998) and can be found in Table 3 along with other model parameters. For the lower mantle + metallic outer core model, a 30% non-modal partial melt was generated from a spinel peridotite containing a minimum of 0.1 and a maximum of 0.5 wt.% outer core, which we assume was exhausted. The crystal fractionation sequence was the same as that used in the upper and lower mantle models (see Fig. 10A and B). The PGE profiles of the primary and fractionated melts produced span the range of the OJP basalt compositions analyzed in this study, although Pt/Ru ratios are more fractionated in the model compositions (Fig. 10C).

The OIB-type basalt, WHTO-36, is a potential representative of the OJP plume tail and should therefore contain the most undiluted signature of the ultimate source, presumably lower mantle and outer core. For this model, melting was again conducted in the spinel peridotite stability field with a maximum degree of partial melting of 5% followed by three stages of fractional crystallization using known sequences for tholeiitic OIBs from the literature (e.g., Hughes, 1982; Wilson, 1989); each stage crystallizes 5% of the magma (see Fig. 10 for details). Note that the PGE profile of the OIB-type basalt WHTO-36 is approximated from a minimum of 0.6% to a maximum of 1.0% of an outer core component (we again assume that this component is completely exhausted) mixed with lower mantle containing primitive mantle abundances of the PGEs (Fig. 10D).

4.4.4. A mixed mantle+outer core PGE source for the OJP basalts

In keeping with early models of plume head generation and evolution (cf. Campbell and Griffiths, 1990) and previous modeling of the OJP basalts (Neal et al., 1997), a truly hybrid source containing upper and lower mantle components with variable amounts of outer core material was used in the modeling of OJP basalt PGE contents: 0–1% outer core (Snow and Schmidt, 1998), lower mantle (50.0–49%) and upper mantle (MORB source; 50%) was used, again assuming all melting occurred in the spinel peridotite field (see Fig. 11 for details). The range of compositions between the primary and fractionated melts generated from a source containing no outer core component and one containing 1% outer core spans the range defined by the OJP basalts. As noted by Neal et al. (1997), not all of the OJP basalts have experienced all five stages of fractional crystallization; these would have intermediate PGE profiles between the two extremes mod-

Fig. 10. Modeling of the primitive mantle-normalized PGE patterns from the OJP basalts (A–C) and OIB-type basalt WHTO-36 (D). The OJP basalt field in (A–C) shows the range of normalized PGE values that these basalts cover and the average PGE profile is calculated from Table 2. The retention of Cr-rich spinel in the source or its removal during fractional crystallization produces $[Ir/Ru]_{PM}$ values that are >1, just as are observed for many of the OJP basalts. Primitive mantle values are from McDonough and Sun (1995). (A) An upper mantle source composition for the OJP basalts. The source used was the spinel peridotite residue after MORB extraction (see Fig. 9) and the mineralogy was taken to be 67.7% olivine, 16.7% clinopyroxene, 3.3% spinel and 12.3% orthopyroxene, with melting proportions of 35:25:5:35, respectively. The primary magma generated by a minimum of 10% and a maximum of 30% partial melting was subject to five stages of fractional crystallization (adapted from Neal et al., 1997): Stage 1 = 100% olivine; Stage 2 = 95% olivine + 5% spinel (chromite); Stage 3 = 50% olivine + 50% clinopyroxene; Stage 4 = 95% clinopyroxene + 5% plagioclase; Stage 5 = 89.5% clinopyroxene + 5% plagioclase + 5% orthopyroxene + 0.5% titanomagnetite. Each stage crystallizes 10% of the magma. (B) A lower mantle source composition for the OJP basalts. A spinel peridotite source was again used, with a mineralogy of 64.94% olivine, 18% clinopyroxene, 4% spinel, 13% orthopyroxene and 0.06% sulfide melting in the proportions 37.4:32:10:20:0.6, respectively. The fractional crystallization sequence described for (A) was applied to the primary magma, which was generated by a minimum of 10% and a maximum of 30% partial melting. (C) A lower mantle + outer core source composition for the OJP basalts. Two source compositions were used containing 0.1% and 0.5% of outer core material (see Table 3). Spinel peridotite sources were used, with a mineralogy of 64.84–64.44% olivine, 10% clinopyroxene, 5% spinel, 26% orthopyroxene, 0.06% sulfide and 0.1–0.5% metal melting in the proportions (36.4–27.4):32:10:20:0.6:(1–5), respectively. The fractional crystallization sequence described for (A) was applied to each primary magma, each generated by 30% partial melting. (D) A lower mantle + outer core model for the PGE composition of OIB-type basalt WHTO-36. This OIB-type sample could be a manifestation of the tail from the OJP plume and melts have been generated from source compositions containing 0.6% and 1% of outer core material added to a lower mantle composition, with melting occurring in the spinel peridotite stability field. The source mineralogy used in this modeling was 63.94–64.34% olivine, 18% clinopyroxene, 4% spinel, 13% orthopyroxene, 0.06% sulfide, and 0.6–1.0% metal (outer core) melting in the proportions (35–43):23.8:10:10:1.2:(12–20), respectively. The primary magmas were generated by 5% partial melting and were subject to three stages of fractional crystallization: Stage 1 = 100% olivine; Stage 2 = 70% olivine + 30% plagioclase; Stage 3 = 94.7% clinopyroxene + 5% plagioclase + 0.3% titanomagnetite. Each stage crystallizes 5% of the magma.

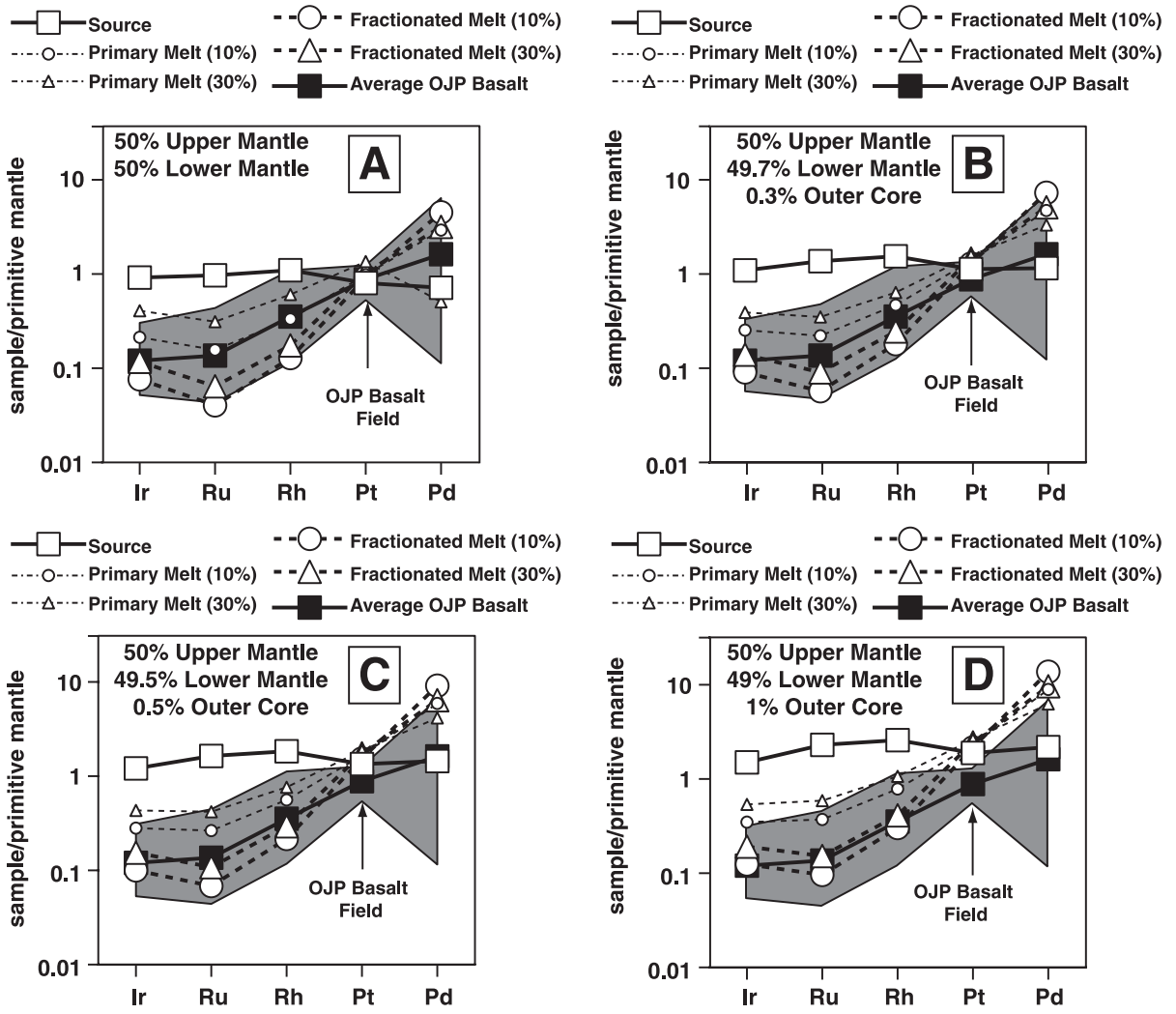

Fig. 11. Modeling of the primitive mantle-normalized PGE patterns from the OJP basalts using a hybrid source. The OJP basalt field in (A–D) shows the range of normalized PGE values that these basalts cover and the average PGE profile is calculated from Table 2. Primitive mantle values are from McDonough and Sun (1995). Spinel peridotite sources were used, with a mineralogy of 64.94–64.44% olivine, 18% clinopyroxene, 4% spinel, 13% orthopyroxene 0.06% sulfide and 0–0.5% metal melting in the proportions (37.4–32.4):32:10:20:0.6:(0–5), respectively. The primary melts are generated by 10% and 30% partial melting and the fractional crystallization scheme described for the OJP basalts in Fig. 10 was also used here. See Table 3 for source compositions. (A) source = 50% upper mantle + 50% lower mantle; (B) source = 50% upper mantle + 49.7% lower mantle + 0.3% outer core; (C) source = 50% upper mantle + 49.5% lower mantle + 0.5% outer core; (D) source = 50% upper mantle + 49 % lower mantle + 1% outer core.

eled in Fig. 11. The results demonstrate that the hybrid source without an outer core component can generate abundances of OJP basalts containing the lowest amounts of PGEs (Fig. 11A). As progressively higher proportions of outer core components are added, the OJP basalt PGE range is reproduced (Fig. 11B–D).

4.4.5. Observations of ML-475 and ML-476

Petrography and whole-rock major element compositions indicate that OJP basalts ML-475 and ML-476 have accumulated clinopyroxene and titanomagnetite. This may account for their enriched PGE contents relative to the other OJP basalts (Fig. 1B,

Table 2). Using the modeling developed above as a guide, we have conducted simple mixing calculations to model the PGE compositions of ML-475 and ML-476. The PGE abundances in clinopyroxene and titanomagnetite fractionating from the OJP sequence were calculated and added in an iterative process to an average OJP basalt composition (the average taken from basalts not exhibiting a Pd depletion). This simple modeling can generate the observed Ir, Ru, Rh and Pt abundances of both samples (Fig. 12), but Pd abundances are underestimated in both cases. The underestimation of Pd may reflect that the Pd K_ds used are low, that the samples not exhibiting a Pd depletion may have lost some smaller amount of Pd, or a phase enriched in dominantly Pd (e.g., a metal alloy) has been missed in the petrographic observations. The PGE abundances (except Pd) of ML-475 are generated if the average OJP basalt composition accumulated 35% clinopyroxene and 0.2% titanomagnetite. As a check for this modeling, the major element composition using these parameters was also modeled and reasonable agreement was seen (e.g., CaO and MgO in ML-475 are 14.5 and 9.99 wt.%, while in our model they are 15.0 and 10.1 wt.%, respectively). The modeling of ML-476 was not as coherent. While the PGE pattern for ML-476 was modeled if the average OJP basalt composition accumulated 25% clinopyroxene and 0.15% titanomagnetite (Fig. 12), the major element composition was less coherent (e.g., CaO and MgO are 9.61 and 5.83 wt.%, while in our model they are 10.3 and 7.4 wt.%, respectively, using a ferroan pigeonite clinopyroxene composition).

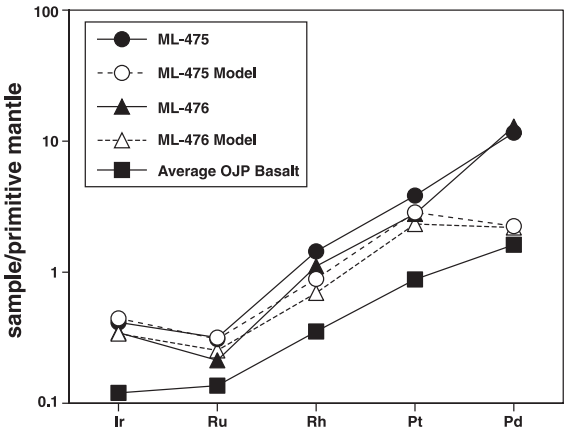

Fig. 12. Results of simple mixing calculations to investigate the cumulate nature of samples ML-475 and ML-476 through accumulation of clinopyroxene and titanomagnetite in an average OJP basalt composition. The clinopyroxene and titanomagnetite PGE compositions are calculated from the fractionating sequence in the model for OJP basalt evolution. The model ML-475 profile is generated by a mixture of 0.2% titanomagnetite, 35% clinopyroxene and 64.8% average OJP basalt, while that of ML-476 is approximated by a mixture of 0.15% titanomagnetite, 25% clinopyroxene and 74.85% average OJP basalt. See text for discussion.

5. Summary, conclusions and future work

The OJP basalts were formed by high degree partial melts (up to 30%) followed by 30–50% fractional crystallization (Mahoney et al., 1993; Neal et al., 1997). The high degree of partial melting would have exhausted any sulfide in the source (>23%; Barnes et al., 1985; Fryer and Greenough, 1992). This precludes any fractionation of the PGEs by retention of sulfide in the source, as may have happened with the Hawaiian picrites (Bennett et al., 2000) that were formed by a lower degree of partial melting.

Both the Singgalo-type and the Kwaimbaita-type of OJP basalt show similar PGE abundances, illustrating at least for the PGEs, a relatively well-mixed source region. Primitive mantle-normalized PGE plots produce smooth patterns with generally positive slopes that result from fractional crystallization, rather than melt generation (Greenough and Fryer, 1995). These patterns are steeper than patterns of other similar high-degree partial melt rocks such as komatiites because of the amount of fractional crystallization experienced by the OJP basalts. Negative Pd anomalies in some OJP patterns, particularly the Singgalo-type basalts, are likely due to the preferential mobility of Pd during low-temperature alteration processes. This is documented in several experimental and field studies, as well as the fact that the Singgalo-type basalts were the last erupted and therefore exposed to more pervasive weathering compared to Kwaimbaita-type basalts, which are deeper in the OJP eruptive stratigraphy. Rare MORB-type and OIB-type basalts were erupted as LIP magmatism waned, and the MORB-type sample may have been contaminated by OJP components but has not undergone sulfide immiscibility. It is unlikely that the OJP basalts have experienced sulfide immiscibility either, based on $[Pt/Y]_{PM}$ vs. $[Y/Cu]_{PM}$ ratios, coupled with low sulfur abundances and the fact

that the OJP basalts are sulfur undersaturated (Michael and Cornell, 1996). Basalts from the deepest part of the OJP stratigraphy on Malaita have accumulated clinopyroxene and titanomagnetite phases (observed petrographically) that account for their elevated PGE abundances relative to other OJP basalts.

The illustrative modeling undertaken in this paper indicates that the MORBs erupted within the OJP sequence contain PGE abundances equally consistent with a derivation from a solely upper mantle source or from a hybrid source dominated by upper mantle material with 20% OJP component (taken to be lower or primitive mantle). The OJP basalts are products of high degrees of partial melting and extensive fractional crystallization. Our modeling suggests that some of them (i.e., those with the lowest PGE abundances) can be derived from a peridotite source that could be upper mantle, lower (primitive) mantle, or a mixture of the two mantle compositions. This is consistent with the $^{187}Os/^{188}Os$ data reported by Parkinson et al. (2001). However, those basalts with elevated PGE abundances cannot be generated from such sources. A source enriched in PGEs above primitive mantle is required to produce these OJP basalts. A hybrid source containing up to 1% of an outer core component, as well as upper and lower mantle components, can adequately model the PGE abundances in the OJP basalts and a similar source containing 0.6–1.0% of an outer core component as well as upper and lower mantle components can generate the PGE composition of OIB-type basalt WHTO-36. The OIB-type sample is taken to represent the tail of the OJP plume (cf. Campbell and Griffiths, 1990). Such a hybrid source is consistent with previous work (Neal et al., 1997) and the inclusion of the outer core component to account for the observed elevated PGE abundances does not adversely impact prior major and trace element modeling.

While recognizing the limitations and model dependency of the partition coefficients (and the assumptions therein) as well as the errors associated with our data, our illustrative modeling indicates that the PGE abundances in *some* of the OJP basalts and the "plume tail" sample, WHTO-36, are consistent with outer core involvement. This work provides further support to a core–mantle boundary origin for at least some of the lavas that form the world's largest LIP. Unequivocal proof of this will be difficult, since analyzing the OJP basalts for $^{186}Os/^{188}Os$ is not possible. However, future work could analyze such basalts for $^{107}Ag/^{109}Ag$ ratios, a parameter that has also been used to define an outer core signature in plume-derived basalts (e.g., Hauri et al., 2000).

Acknowledgements

The people and government of the Solomon Islands are gratefully acknowledged for their support and hospitality during several field seasons to Malaita and Makira. Thoughtful and thorough reviews of this manuscript by Ian Parkinson and Jean-Guy Schilling greatly helped the quality of this paper and they are gratefully thanked for their time and effort. This work was partially supported by NSF grants EAR-93-02471 and EAR-96-28252 to CRN. **[RR]**

References

Alt, J.C., Honnorez, J., Laverne, C., Emmerman, R., 1986. Hydrothermal alteration of a 1 km section through the upper oceanic crust, Deep Sea Drilling Project Hole 504B: mineralogy, chemistry, and evolution of seawater–basalt interactions. J. Geophys. Res. 91, 10309–10335.

Arndt, N.T., 1986. Differentiation of komatiite flows. J. Petrol. 27, 279–301.

Arndt, N.T., Nesbitt, R.W., 1984. Magma mixing in komatiitic lavas from Munro Township, Ontario. In: Kröner, A., et al. (Eds.), Archean Geochemistry. Springer Verlag, Berlin, Heidelberg, pp. 99–114.

Barnes, S.J., Naldrett, A.J., 1986. Variations in platinum group element concentrations in the Alexo mine komatiite. Abitibi greenstone belt, northern Ontario. Geol. Mag. 123, 515–524.

Barnes, S.J., Picard, C.P., 1993. The behavior of platinum-group elements during partial melting, crystal fractionation, and sulfide segregation: an example from the Cape Smith Fold Belt, northern Quebec. Geochim. Cosmochim. Acta 57, 79–87.

Barnes, S.J., Naldrett, A.J., Gorton, M.P., 1985. The origin of the fractionation of platinum-group elements in terrestrial magmas. Chem. Geol. 53, 303–323.

Bender, J.F., Hodges, F.N., Bence, A.E., 1978. Petrogenesis of basalts from the project FAMOUS area: experimental study from 0 to 15 kbars. Earth Planet. Sci. Lett. 41, 277–302.

Bennett, V., Norman, M., Garcia, M., 2000. Rhenium and platinum group element abundances correlated with mantle source components in Hawaiian picrites: sulfides in the plume. Earth Planet. Sci. Lett. 183, 513–526.

Bezmen, N.I., Asif, M., Brügmann, G.E., Romanenko, I.M., Naldrett, A.J., 1994. Distribution of Pd, Rh, Ru, Ir, Os, and Au between sulfide and silicate melts. Geochim. Cosmochim. Acta 58, 1251–1260.

Boehler, R., Chopelas, A., Zerr, A., 1995. Temperature and chemistry of the core–mantle boundary. Chem. Geol. 120, 199–205.

Borisov, A., Palme, H., Spettel, B., 1994. Solubility of palladium in silicate melts: implications for core formation in the Earth. Geochim. Cosmochim. Acta 58, 705–716.

Bowles, J.F.W., Gize, A.P., Vaughan, D.J., Norris, S.J., 1994. Development of platinum-group minerals in laterites—initial comparison of organic and inorganic controls. Trans. Inst. Min. Metall. (Sect. B: Appl. Earth Sci.) 103, B53–B56.

Brandon, A.D., Walker, R.J., Morgan, J.W., Norman, M.D., Prichard, H.M., 1998. Coupled ^{186}Os and ^{187}Os evidence for core–mantle interaction. Science 280, 1570–1573.

Brandon, A.D., Norman, M.D., Walker, R.J., Morgan, J.W., 1999. ^{186}Os–^{187}Os sytematics of Hawaiian picrites. Earth Planet. Sci. Lett. 174, 25–42.

Brügmann, G.E., Arndt, N.T., Hofmann, A.W., Tobschall, H.J., 1987. Noble metal abundances in komatiite suites from Alexo, Ontario, and Gorgona Island, Columbia. Geochim. Cosmochim. Acta 51, 2159–2169.

Brügmann, G.E., Naldrett, A.J., Asif, M., Lightfoot, P.C., Gorbachev, N.S., Fedorenko, V.A., 1993. Siderophile and chalcophile metals as tracers of the evolution of the Siberian Trap in the Noril'sk region, Russia. Geochim. Cosmochim. Acta 57, 2001–2018.

Bryan, W.B., 1983. Systematics of modal phenocryst assemblages in submarine basalts: petrologic implications. Contrib. Mineral. Petrol. 83, 62–74.

Burton, K.W., Gannoun, A., Birck, J.L., Allegre, C.J., Schiano, P., Clocchiatti, R., Alard, O., 2002. The compatibility of rhenium and osmium in natural olivine and their behavior during mantle melting and basalt genesis. Earth Planet. Sci. Lett. 198, 63–76.

Campbell, I.H., Griffiths, R.W., 1990. Implications of mantle plume structure for the evolution of flood basalts. Earth Planet. Sci. Lett. 99, 79–93.

Capobianco, C.J., Hervig, R.L., Drake, M.J., 1990. Effect of iron on Ru, Rh, and Pd crystal/melt partitioning. Eos Trans. AGU 71, F1611 (Fall Meet. Suppl.).

Capobianco, C.J., Drake, M.J., Rogers, S.Z., 1991. Crystal/melt partitioning of Ru, Rh and Pd for silicate and oxide basaltic liquidus phases (abstract). Lunar Planet. Sci. XXII, 179–180.

Capobianco, C.J., Hervig, R.L., Drake, M.J., 1994. Experiments on crystal/liquid partitioning of Ru, Rh and Pd for magnetite and hematite solid solutions crystallized from silicate melt. Chem. Geol. 113, 23–43.

Coffin, M.F., Eldholm, O., 1993. Large igneous provinces. Sci. Am., 42–49 (Oct.).

Coleman, P.J., Kroenke, L.W., 1981. Subduction without volcanism in the Solomon Islands arc. Geo-Mar. Lett. 1, 129–134.

Crocket, J.H., MacRae, W.E., 1986. Platinum group element distribution in komatiitic and tholeiitic volcanic rocks from Munro Township, Ontario. Econ. Geol. 81, 1242–1251.

Devey, C.W., Garbe-Schönberg, C.D., Stoffers, P., Chauvel, C., Mertz, D.F., 1994. Geochemical effects of dynamic melting beneath ridges: reconciling major and trace element variations in Kolbeinsey (and global) mid-ocean ridge basalt. J. Geophys. Res. 99 (B5), 9077–9095.

de Wijs, G.A., Kresse, G., Vocadlo, L., Dobson, D., Alfe, D., Gillan, M.J., Price, G.D., 1998. The viscosity of liquid iron at the physical conditions of the Earth's core. Nature 392, 805–807.

Ely, J.C., Neal, C.R., 2002. Method of data reduction and uncertainty estimation for platinum-group element data using inductively coupled plasma-mass spectrometry. Geostand. Newsl. 26, 31–39.

Ely, J.C., Neal, C.R., O'Neill Jr., J.A., Jain, J.C., 1999. Quantifying the platinum group elements (PGEs) and gold in geological samples using cation exchange pretreatment and ultrasonic nebulization inductively coupled plasma mass spectrometry (USN-ICP-MS). Chem. Geol. 157, 219–234.

Fleet, M.E., Stone, W.E., 1991. Partitioning of platinum-group elements in the Fe–Ni–S system and their fractionation in nature. Geochim. Cosmochim. Acta 55, 245–253.

Fleet, M.E., Stone, W.E., Crocket, J.H., 1991. Partitioning of Pd, Ir, and Pt between sulfide liquid and basalt melt: effects of melt composition, concentration, and oxygen fugacity. Geochim. Cosmochim. Acta 55, 2545–2554.

Fleet, M.E., Crocket, J.H., Stone, W.E., 1994. Sulphide/silicate melt partition coefficients for platinum-group elements and gold (abstract). V.M. Goldschmidt Conference, Edinburgh, Min. Mag, vol. 58 A, pp. 276–277.

Fleet, M.E., Crocket, J.H., Liu, M., Stone, W.E., 1999. Laboratory partitioning of platinum-group elements (PGE) and gold with application to magmatic sulfide–PGE deposits. Lithos 47, 127–142.

Fryer, B.J., Greenough, J.D., 1992. Evidence for mantle heterogeneity from platinum-group-element abundances in Indian Ocean basalts. Can. J. Earth Sci. 29, 2329–2340.

Greenough, J.D., Fryer, B.J., 1990. Distribution of gold, palladium, platinum, rhodium, ruthenium, and iridium in Leg 115 hotspot basalts: implications for magmatic processes. Proc. ODP Sci. Res. 115, 71–84.

Greenough, J.D., Fryer, B.J., 1995. Behavior of the platinum-group elements during differentiation of the North Mountain basalt, Nova Scotia. Can. Mineral. 33, 153–163.

Handler, M.R., Bennett, V.C., 1999. Behavior of platinum group elements in the subcontinental mantle of eastern Australia during variable metasomatism and melt depletion. Geochim. Cosmochim. Acta 63, 3597–3618.

Hauri, E.H., Lassiter, J.C., DePaolo, D.J., 1996. Osmium isotope systematics of drilled lavas from Mauna Loa, Hawaii. J. Geophys. Res. 101 (B5), 11793–11806.

Hauri, E.H., Carlson, R.W., Bauer, J., 2000. The timing of core formation and volatile depletion in solar system objects from high-precision ^{107}Pd–^{107}Ag isotope systematics. Lunar Planet. Sci., vol. XXXI. Lunar and Planetary Institute, Houston. Abstract #1812; CD-ROM.

Helmberger, D.V., Wen, L., Ding, X., 1998. Seismic evidence that the source of the Iceland hotspot lies at the core–mantle boundary. Nature 396, 251–255.

Hemond, C., Arndt, N.T., Lichtenstein, U., Hofmann, A.W., 1993. The heterogeneous Iceland plume: Nd–Sr–O isotopes and trace element constraints. J. Geophys. Res. 98 (B9), 15833–15850.

Holzheid, A., Grove, T.L., 2002. Sulfur saturation limits in silicate melts and their implications for core formation scenarios for terrestrial planets. Am. Mineral. 87, 227–237.

Hughes, C.J., 1982. Igneous Petrology. Developments in Petrology, vol. 7. Elsevier, New York. 551 pp.

Jones, J., Drake, M.J., 1986. Geochemical constraints on core formation in the Earth. Nature 322, 221–228.

Kellogg, L.H., King, S.D., 1993. Effect of mantle plumes on the growth of D″ by reaction between the core and mantle. Geophys. Res. Lett. 20, 379–382.

Lightfoot, P.C., Naldrett, A.J., Gorbachev, N.S., Doherty, W., Fedorenko, V.A., 1990. Geochemistry of the Siberian Trap of the Noril'sk area, USSR, with implications for the relative contributions of crust and mantle to flood basalt magmatism. Contrib. Mineral. Petrol. 104, 631–644.

Mahoney, J.J., Spencer, K.J., 1991. Isotopic evidence for the origin of the Manihiki and Ontong Java oceanic plateaus. Earth Planet. Sci. Lett. 104, 196–210.

Mahoney, J.J., Storey, M., Duncan, R.A., Spencer, K.J., Pringle, M., 1993. Geochemistry and age of the Ontong Java Plateau. In: Pringle, M.S., et al. (Eds.), The Mesozoic Pacific: Geology, Tectonics, and Volcanism. AGU Geophys. Monogr. Ser., vol. 77, pp. 233–262.

Malvin, D.J., Drake, M.J., Benjamin, T.M., Duffy, C.J., Hollander, M., Rogers, P.S.Z., 1986. Experimental partitioning studies of siderophile elements amongst lithophile phases: preliminary results using PIXE microprobe analysis (abstract). Lunar Planet. Sci. XVII, 514–515.

McCandless, T.E., Ruiz, J., Adair, B.I., Freydier, C., 1999. Re–Os isotope and Pd/Ru variations in chromitites from the Critical Zone Bushveld Complex, South Africa. Geochim. Cosmochim. Acta 63, 911–923.

McDonald, I., De Wit, M.J., Smith, C.B., Bizzi, L.A., Viljoen, K.S., 1995. The geochemistry of the platinum-group elements in Brazilian and southern African kimberlites. Geochim. Cosmochim. Acta 59, 2883–2903.

McDonough, W.F., Sun, S., 1995. The composition of the Earth. Chem. Geol. 120, 223–253.

McKenzie, D., O'Nions, R.K., 1991. Partial melt distributions from inversion of rare earth element concentrations. J. Petrol. 32, 1021–1091.

Michael, P.J., 1999. Implications for magmatic processes at Ontong Java Plateau from volatile and major element contents of Cretaceous basalt glasses. Geochem. Geophys. Geosys. 1 (Paper number 1999GC000025).

Michael, P.J., Cornell, W.C., 1996. H_2O, CO_2, Cl, and S contents in 122 Ma glasses from Ontong Java Plateau, ODP 807C: implications for mantle and crustal processes. Eos Trans. AGU 77, F714 (Fall Meet Suppl.).

Mitchell, R.H., Keays, R.R., 1981. Abundance and distribution of gold, palladium and iridium in some spinel and garnet lherzolites: implications for the nature and origin of precious metal-rich intergranular components in the upper mantle. Geochim. Cosmochim. Acta 45, 2425–2442.

Mountain, B.W., Wood, S.A., 1988. Solubility and transport of platinum-group elements in hydrothermal solutions' thermodynamic and physical chemical constraints. In: Prichard, H.M., et al. (Eds.), Geo-Platinum '87. Elsevier, New York, pp. 57–82.

Neal, C.R., 1986. Mantle studies in the western Pacific and kimberlite-type intrusives. Unpub. PhD thesis, University of Leeds, UK. 365 pp.

Neal, C.R., 2001. Interior of the moon: the presence of garnet in the primitive deep lunar mantle. J. Geophys. Res. 106, 27865–27885.

Neal, C.R., Mahoney, J.J., Kroenke, L.W., Duncan, R.A., Petterson, M.G., 1997. The Ontong Java Plateau. In: Mahoney, J.J., Coffin, M.F. (Eds.), Large Igneous Provinces: Continental, Oceanic, and Planetary Flood Volcanism. AGU Geophys. Monogr. Ser., vol. 100, pp. 183–216.

Norman, M.D., Garcia, M.O., 1999. Primitive magmas and source characteristics of the Hawaiian plume: petrology and geochemistry of shield picrites. Earth Planet. Sci. Lett. 168, 27–44.

Norrish, K., Chappell, B.W., 1977. X-ray fluorescence spectrometry. In: Zussman, J. (Ed.), Physical Methods in Determinative Mineralogy. Academic Press, New York, pp. 201–272.

Parkinson, I.J., Schaefer, B.F., OJP Leg 192 Shipboard Scientific Party, 2001. A lower mantle origin for the world's biggest LIP? A high precision Os isotope isochron from Ontong Java Plateau basalts drilled on OJP Leg 192. Eos Trans. AGU 82 (47), F1398 (Fall Meet. Suppl.).

Petterson, M.G., 1995. The geology of North and Central Malaita, Solomon Islands (including implications of Geological Research on Makira, Savo Island, Guadalcanal, and Choiseul between 1992 and 1995). Geological Mem. 1/95. Water and Mineral Resources Division, Ministry of Energy, Water, and Mineral Resources, Honiara, Solomon Islands. 219 pp.

Petterson, M.G., Babbs, T., Neal, C.R., Mahoney, J.J., Saunders, A.D., Duncan, R.A., Tolia, D., Magu, R., Qopoto, C., Mahoa, H., Natogga, D., 1999. Geological–tectonic framework of Solomon Islands, SW Pacific: crustal accretion and growth within an intra-oceanic setting. Tectonophysics 301, 35–60.

Prichard, H.M., Lord, R.A., 1990a. Platinum and palladium in the Troodos ophiolite complex, Cyprus. Can. Mineral. 28, 607–617.

Prichard, H.M., Lord, R.A., 1990b. Evidence for differential mobility of platinum-group elements in the secondary environment in Shetland ophiolite complex. Trans. Inst. Min. Metall. (Sect. B: Appl. Earth Sci.) 103, B79–B86.

Puchtel, I.S., Humayun, M., 2001. Platinum group element fractionation in a komatiitic basalt lava lake. Geochim. Cosmochim. Acta 65, 2979–2993.

Puchtel, I.S., Hofmann, A.W., Mezger, K., Shchipansky, A.A., Kulikov, V.S., Kuikova, V.V., 1996. Petrology of a 2.41 Ga remarkably fresh komatiitic basalt lava lake in Lion Hills, central Vetreny Belt, Baltic Shield. Contrib. Mineral. Petrol. 124, 273–290.

Rehkämper, M., Halliday, A.N., Barfod, D., Fitton, J.G., Dawson, J.B., 1997. Platinum-group element abundance patterns in different mantle environments. Science 278, 1595–1598.

Rehkämper, M., Halliday, A.N., Fitton, J.G., Lee, D.C., Wieneke, M., Arndt, N.T., 1999. Ir, Ru, Pt, and Pd in basalts and komatiites: new constraints for the geochemical behavior of the platinum-group elements in the mantle. Geochim. Cosmochim. Acta 63, 3915–3934.

Richards, M.A., Duncan, R.A., Courtillot, V.E., 1989. Flood basalts and hot-spot tracks: plume heads and tails. Science 246, 103–107.

Richardson, W.P., Okal, E.A., van der Lee, S., 2000. Rayleigh-wave tomography of the Ontong Java Plateau. Phys. Earth Planet. Int. 118, 29–51.

Righter, K., 1999. Experimental constraints on the behavior of rhenium and osmium during mantle melting and magmatic differentiation. Ninth Annual V.M. Goldschmidt Conference, Abstract #7530. LPI Contribution No. 971. Lunar and Planetary Institute, Houston CD-ROM.

Righter, K., Hauri, E.H., 1998. Compatibility of rhenium in garnet during mantle melting and magma genesis. Science 280, 1737–1741.

Righter, K., Walker, R.J., Warren, P.H., 2000. Significance of highly siderophile elements and osmium isotopes in the lunar and terrestrial mantles. Origin of the Earth and Moon. Univ. Arizona Press, Tucson, AZ, pp. 291–322.

Roy-Barman, M., Wasserburg, G.J., Papanastassiou, D.A., Chaussidon, M., 1998. Osmium isotopic compositions and Re–Os concentrations in sulfide globules from basaltic glasses. Earth Planet. Sci. Lett. 154, 331–347.

Russell, S.S., Lay, T., Garnero, E.J., 1998. Seismic evidence for small-scale dynamics in the lowermost mantle at the root of the Hawaiian hotspot. Nature 396, 255–258.

Salpeteur, I., Jezequel, J., 1992. Platinum and palladium stream-sediment geochemistry downstream from PGE-bearing ultramafics, West Andriamena area, Madagascar. J. Geochem. Explor. 43, 43–65.

Snow, J.E., Schmidt, G., 1998. Constraints on Earth accretion deduced from noble metals in the oceanic mantle. Nature 391, 166–169.

Sun, S., 1982. Chemical composition and origin of the Earth's primitive mantle. Geochim. Cosmochim. Acta 46, 179–192.

Tatsumi, Y., Oguri, K., Shimoda, G., 1999. The behavior of platinum-group elements during magmatic differentiation in Hawaiian tholeiites. Geochem. J. 33, 237–247.

Taufen, P.M., Marchetto, C.M.L., 1989. Tropical weathering control of Ni, Cu, Co, and platinum group element distributions at the O'Toole Ni–Cu sulphide deposit, Minas Gerais, Brazil. J. Geochem. Explor. 32, 185–197.

Tejada, M.L.G., Mahoney, J.J., Duncan, R.A., Hawkins, M.P., 1996. Age and geochemistry of basement and alkalic rocks of Malaita and Santa Isabel, Solomon Islands, southern margin of Ontong Java Plateau. J. Petrol. 37, 361–394.

Tejada, M.L.G., Mahoney, J.J., Neal, C.R., Duncan, R.A., Petterson, M.G., 2002. Basement geochemistry and geochronology of central Malaita, Solomon Islands, with implications for the origin and evolution of the Ontong Java Plateau. J. Petrol. 43, 449–484.

Tredoux, M., Lindsay, N.M., Davies, G., McDonald, I., 1995. The fractionation of platinum group elements in magmatic systems, with the suggestion of a novel causal mechanism. South Afr. J. Geol. 98, 157–167.

Van Dyke, A., 2000. A geochemical investigation of San Cristobal (Makira) basement: evidence for the presence of Ontong Java Plateau crust. Unpub. PhD thesis, University of Notre Dame. Notre Dame.

Vatin-Perignon, N., Amossé, J., Radelli, L., Keller, F., Catro Layva, T., 2000. Platinum group element behavior and thermochemical constraints in the ultrabasic–basic complex of the Vizcaino Peninsula, Baja California Sur, Mexico. Lithos 53, 59–80.

Vinnik, L., Breger, L., Romanowicz, B., 1998. Anisotropic structures at the base of the Earth's mantle. Nature 393, 564–567.

Walker, D., Shibata, T., Delong, S.E., 1979. Abyssal tholeiites from Oceanographer Fracture Zone II. Phase equilibria and mixing. Contrib. Mineral. Petrol. 70, 111–125.

Walker, R.J., Morgan, J.W., Horan, M.F., 1995. Osmium-187 enrichment in some plumes: evidence for core–mantle interaction? Science 269, 819–822.

Walker, R.J., Morgan, J.W., Beary, E.S., Smoliar, M.I., Czamanske, G.K., Horan, M.F., 1997. Applications of the $^{190}Pt-^{186}Os$ isotope system to geochemistry and cosmochemistry. Geochim. Cosmochim. Acta 61, 4799–4807.

Walter, M.J., Newsom, H.E., Ertel, W., Holzheid, A., 2000. Siderophile elements in the Earth and Moon: metal/silicate partitioning and implications for core formation. Origin of the Earth and Moon. Univ. Arizona Press, Tucson, AZ, pp. 265–289.

Wen, L., Helmberger, D.V., 1998. Ultra-low velocity zones near the core–mantle boundary from broadband PKP precursors. Science 279, 1701–1703.

Wendlandt, R.F., 1982. Sulfide saturation of basalt and andesite melts at high pressures and temperatures. Am. Mineral. 67, 877–885.

Wilson, M., 1989. Igneous Petrogenesis. Unwin Hyman, Boston, MA. 466 pp.

Wood, S.A., 1990. The interaction of dissolved platinum with fulvic acid and simple organic acid analogues in aqueous solutions. Can. Mineral. 28, 665–673.

Wood, S.A., Vlassopoulos, D., 1990. The dispersion of Pt, Pd and Au in surficial media about two PGE–Cu–Ni prospects in Quebec. Can. Mineral. 28, 649–663.

Zhou, M.-F., Sun, M., Keays, R.R., Kerrich, R., 1998. Controls on platinum group elemental distributions of podiform chromitites: a case study of high-Cr and high-Al chromitites from Chinese orogenic belts. Geochim. Cosmochim. Acta 62, 677–688.